# **Journal Name**

# **ARTICLE TYPE**

Cite this: DOI: 00.0000/xxxxxxxxxx

# Effects of State Filling and Localization on Chemical Expansion in Praseodymium-Oxide Perovskites

Adrian Xiao Bin Yong, ab Lawrence O. Anderson, ab Nicola H. Perry and Elif Ertekin\*bc

Received Date Accepted Date

DOI: 00.0000/xxxxxxxxxx

In oxide materials, an increase in oxygen vacancy concentration often results in lattice expansion, a phenomenon known as chemical expansion that can introduce detrimental stresses and lead to potential device failure. One factor often implicated in the chemical expansion of materials is the degree of localization of the multivalent cation electronic states. When an oxygen  $O_{O}^{\times}$  is removed from the lattice and a vacancy vo forms, it is believed that the two released electrons reduce multivalent cations and expand the lattice, with more localized cation states resulting in larger expansion. In this work, we computationally and experimentally studied the chemical expansion of two Pr-based perovskites that exhibit ultra-low chemical expansion,  $PrGa_{1-x}Mg_xO_{3-\delta}$  and  $BaPr_{1-x}Y_xO_{3-\delta}$ , and their parent compounds  $PrGaO_{3-\delta}$  and  $BaPrO_{3-\delta}$ . Using density functional theory, the degree of localization of the Pr-4f electrons was varied by adjusting the Hubbard U parameter. We find that the relationship between Pr-4f electron localization and chemical expansion exhibits more complexity than previously established. This relationship depends on the nature of the states filled by the two electrons, which may not necessarily involve the reduction of Pr. F'-center defects can form if the reduction of Pr is unfavorable, leading to smaller chemical expansions. If hole states are present in the material, the states filled by the electrons can be Pr-4f and/or O-2p hole states depending on the degree of Pr-4f localization. The O-2p holes are more delocalized than the Pr-4f holes, resulting in smaller chemical expansions when the O-2p holes are filled. X-ray photoelectron spectroscopy reveals low concentrations of  $Pr^{4+}$  in  $PrGa_{0.9}Mg_{0.1}O_{3-\delta}$  and  $BaPr_{0.9}Y_{0.1}O_{3-\delta}$ , supporting the possible role of O-2p holes in the low chemical expansions exhibited by these materials. This work highlights the non-trivial effects of electron localization on chemical expansion, particularly when hole states are present, pointing to design strategies to tune the chemical expansion of materials.

#### 1 Introduction

Oxide materials used in solid oxide fuel cells (SOFCs), oxygen permeation membranes, and ceramic oxygen generators (COGs) <sup>1,2</sup> are subjected to changes in temperature and oxygen partial pressure during synthesis, device startup, shutdown, and operation, leading to changes in oxygen stoichiometry. These changes in oxygen stoichiometry alter the lattice parameters of the materials, a phenomenon known as chemical expansion <sup>3,4</sup>. Chemical expansion can occur across a wide range of oxide materials, e.g., perovskites <sup>5</sup>, fluorites <sup>6</sup>, Ruddlesden-Popper structures <sup>7</sup>, and hexagonal manganites <sup>8</sup>. Battery electrodes are an-

<sup>a</sup> Department of Materials Science and Engineering, University of Illinois Urbana-

behind chemical expansion such that strategies can be developed to tune the chemical expansion of materials. Although chemical expansion may be caused by phase changes arising from changes in stoichiometry, the subject of this study is the chemical expansion that occurs in the absence of phase changes. This chemical expansion is described mathematically for a perovskite of chemical formula  $ABO_{3-\delta}$ , assuming linear behavior, as

other notable group of materials that can demonstrate chemical expansion with changes in stoichiometry of Li, Na, etc<sup>9</sup>. In these

applications, small chemical expansion is desired to reduce me-

chanical degradation and prevent potential failure  $^{10,11}$ . On the

other hand, there are emerging applications where large chemi-

cal expansion is desired, such as electro-chemo-mechanical actua-

$$\varepsilon = \frac{a - a_0}{a_0} = \alpha_C \Delta \delta \quad , \tag{1}$$

where  $\varepsilon$  is the isothermal lattice strain, a and  $a_0$  are the final

alter the lattice parameters of own as chemical expansion <sup>3,4</sup>.

ross a wide range of oxide maes <sup>6</sup>, Ruddlesden-Popper struces <sup>8</sup>. Battery electrodes are anAlthough chemical expansion may be caused by phase changes

Champaign, Urbana, Illinois, USA.

<sup>b</sup> Materials Research Laboratory, University of Illinois Urbana-Champaign, Urbana, Illinois. USA.

<sup>&</sup>lt;sup>c</sup> Department of Mechanical Science and Engineering, University of Illinois Urbana-Champaign, Urbana, Illinois, USA. Email: ertekin@illinois.edu

<sup>†</sup> Electronic Supplementary Information (ESI) available: [details of any supplementary information available should be included here]. See DOI: 00.0000/00000000.

and initial lattice parameters respectively,  $\alpha_C$  is the coefficient of chemical expansion (CCE), and  $\Delta\delta$  is the change in oxygen content per formula unit. A simple model has been proposed to explain the atomistic origins of chemical expansion  $^{15-17}$ . When an oxygen vacancy  $\mathbf{v}_0^{\bullet\bullet}$  forms, two electrons are released into the oxide. These electrons are often assumed to reduce the cations in the oxide. As such, chemical expansion is believed to be caused by two competing effects: (1) lattice expansion due to increase in ionic radius of the reduced cations and (2) lattice contraction around the oxygen vacancies due to electrostatic interactions. The former effect is often more significant than the latter, resulting in a net lattice expansion.

Based on this framework, one of the factors affecting chemical expansion is the degree of localization of the electronic states of the multivalent cation in the material. Marrocchelli et al.  $^{18}$  performed a computational study of the chemical expansion of  $\text{CeO}_{2-\delta}$  and  $\text{BaCeO}_{3-\delta}$ , in which the Ce-4f orbitals are filled upon cation reduction. They found that the higher the degree of localization of the Ce-4f electrons, the higher the CCEs of both materials. This finding was attributed to a larger increase in volume when the electrons localize on a few Ce cations, as compared to when the electrons are delocalized throughout many Ce cations resulting in only slight increases in cation radii overall. Subsequent experimental studies on  $(\text{La,Sr})(\text{Ga,Ni})\text{O}_{3-\delta}$  (LSGN)  $^{19,20}$  and  $\text{SrTi}_{1-x}\text{Fe}_x\text{O}_{3-\delta}$  (STF)  $^5$  confirmed that higher charge localization (of Ni and Fe respectively) corresponded to higher CCEs.

However, the relationship between the cation electron localization and chemical expansion may not be so straightforward, if for example the multivalent cation is not reduced during O removal. A computational study  $^{21}$  on  $\rm ATiO_3$  (A = Ca, Sr, Ba) found that the chemical expansion can decrease as the Ti electrons become more localized, due to the electrons localizing on the O vacancy site instead of reducing Ti ions. The vast majority of computational studies examine chemical expansion in the absence of hole states, which usually results in the reduction of multivalent cations and leaves the effects of hole states and their localized/delocalized nature on chemical expansion underexplored.

In our recent work<sup>22</sup>, we reported the discovery of unprecedented near-zero CCEs for two Pr-based perovskites,  $PrGa_{1-x}Mg_xO_{3-\delta}$  (PGM) and  $BaPr_{1-x}Y_xO_{3-\delta}$  (BPY). These low CCEs are unexpected in materials where oxygen vacancies are believed to be compensated by reduction of Pr cations, via filling of localized 4f hole states. Here, we present an in-depth computational and experimental study of the chemical expansion of these Pr-based perovskites, PGM and BPY, and their parent compounds  $PrGaO_{3-\delta}$  (PGO) and  $BaPrO_{3-\delta}$  (BPO), to identify possible reasons underlying their ultra-low CCEs and new insights that can be gained about chemical expansion. Using density functional theory (DFT), we show that the relationship between localization of the 4f cation orbitals and chemical expansion is not straightforward, and it depends on the type of electronic state that is filled when oxygen is removed. For cases where hole states are present, the relationship diverges from previous understanding. Since the hole states become filled when oxygen is removed, it is the degree of localization of the hole states that directly affects the chemical expansion, which does not necessarily correlate with the degree of localization of the multivalent cation electrons. Localization of the Pr-4f electrons non-intuitively leads to the formation of O-2p, instead of Pr-4f, hole states, where the O-2p hole states are more delocalized and thus give smaller chemical expansions. X-ray photoelectron spectroscopy (XPS) is used to probe the type of hole states present in PGM and BPY to help connect our theoretical understanding to experimental behavior. The low  $Pr^{4+}$  contributions to the Pr spectra are supportive of the presence of  $Pr^{4+}$  contributions to the Pr spectra are supportive of the presence of  $Pr^{4+}$  contributions in these materials which exhibit ultra-low CCEs. This work sheds light on the complexities that can arise when the multivalent cations are not simply reduced during chemical expansion, and the opportunities these complexities can bring to tuning chemical expansion.

# 2 Methods

#### 2.1 Computational methods

All DFT calculations were performed using the Vienna Ab initio Simulation Package (VASP)  $^{23-26}$ , with the projector augmented-wave (PAW) method  $^{27,28}$ . The Pr  $(5s^2\ 5p^6\ 5d^1\ 4f^2\ 6s^2)$ , Ga  $(3d^{10}\ 4s^2\ 4p^1)$ , Mg  $(3s^2)$ , Ba  $(5s^2\ 5p^6\ 6s^2)$ , Y  $(4s^2\ 4p^6\ 4d^2\ 5s^1)$ , and O  $(2s^2\ 2p^4)$  electrons were treated as valence electrons in the pseudopotentials. The generalized gradient approximation (GGA) with the Perdew-Burke-Ernzerhof (PBE) exchange-correlation functional  $^{29}$  was used, and the orbitals were expanded using a plane wave basis with cutoff energy of 520 eV. Structural relaxation was performed on all structures, allowing the cell shape, cell volume, and atom positions to relax, until the force on each atom was below 0.01 eV/Å.

Localized states such as the 4f orbitals of Pr are typically not described well by standard DFT functionals, due to the selfinteraction error  $^{30}$ . Many d- and f-block elements face this issue, and a commonly used solution is the DFT+U method<sup>31-33</sup>, which includes a Hubbard U term in the Hamiltonian. The Uvalue is typically tuned to more properly describe the degree of electron localization and provide a more accurate material description. The U value can also be varied to study chemical expansion over a range of electron localizations, as carried out in previous computational studies <sup>18,21</sup>. Prior to our work, no systematic Hubbard U study of the Pr-4f states for our Pr-based perovskites had been performed. Therefore, we studied the chemical expansion of our Pr-based perovskites over varying U in order to identify physically reasonable U values for our materials. As a natural consequence, we were also able to study the relationship between Pr-4f electron localization and chemical expansion. The DFT+U method based on Dudarev's approach 34 was used to treat the on-site Coulomb interaction of the Pr-4f electrons, where the U value was varied from 0 to 10 eV in 2 eV intervals.

Our materials were studied in their respective crystal structures corresponding to the temperature range of the experiments  $^{22}$  (700–900 °C). PrGaO<sub>3</sub> adopts the orthorhombic *Pbnm* space group, as shown in Fig. 1a, throughout the temperature range  $^{35}$ . On the other hand, BaPrO<sub>3</sub> undergoes a phase transition from rhombohedral  $R\overline{3}c$  to cubic  $Pm\overline{3}m$  around 860 °C <sup>36</sup>, and we chose to study it in the cubic space group (see Fig. 1b) for simplicity. The same crystal structures were adopted for the

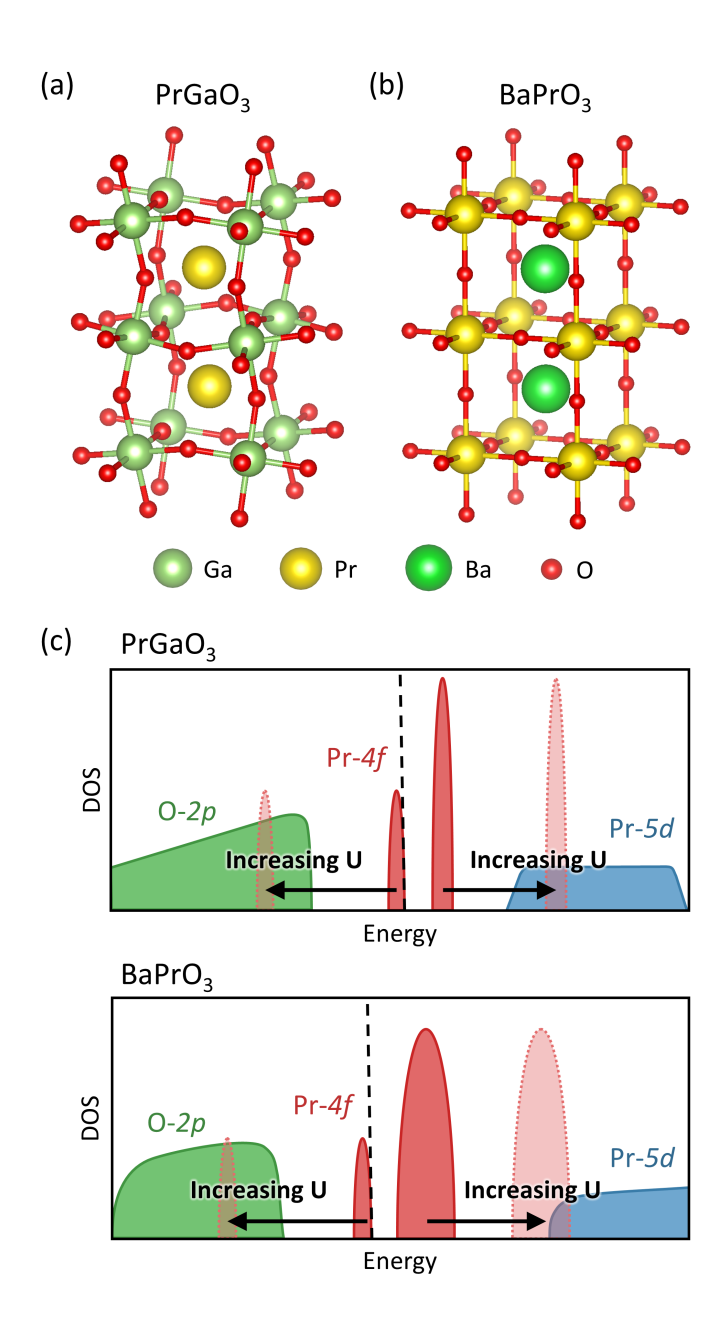


**Fig.** 1 Crystal structure of (a)  $PrGaO_3$  with space group Pbnm and (b)  $BaPrO_3$  with space group  $Pm\overline{3}m$ . Pr occupies the A-site in  $PrGaO_3$  and the B-site in  $BaPrO_3$ . The  $BO_6$  octahedra in the orthorhombic  $PrGaO_3$  are tilted compared to the cubic  $BaPrO_3$ . (c) Simplified depiction of the PDOS of  $PrGaO_3$  and  $BaPrO_3$ , where the black dashed line represents the Fermi level. As the U value increases, the occupied Pr-4f states shift to lower energies, whereas the unoccupied Pr-4f states shift to higher energies.

doped form of the materials (x = 0.125), as the crystal structures are not expected to change for the given level of doping <sup>36,37</sup>. Fig. 1c shows how the energy levels of the Pr-4f states change as the Hubbard U value is increased (i.e., as the Pr-4f electrons become more localized), using simplified representations of the projected density of states (PDOS) for PrGaO<sub>3</sub> and BaPrO<sub>3</sub> (see ESI Fig. S1 for actual PDOS). In both cases, the occupied Pr-4f states shift down in energy towards the O-2p states, whereas the unoccupied Pr-4f states shift up in energy towards the Pr-5d states.

Simulations for  $PrGa_{1-x}Mg_xO_{3-\delta}$  and  $BaPr_{1-x}Y_xO_{3-\delta}$  (x=0, 0.125) were performed using  $2 \times 2 \times 1$  and  $2 \times 2 \times 4$  unit cells respectively; both correspond to 80 atom supercells. The Brillouin zone was sampled using a  $(2 \times 2 \times 2)$  Monkhorst-Pack k-point grid in all cases. In both materials, the acceptor-doped compositions corresponding to x = 0.125 were achieved by replacing two B-site atoms with dopant atoms. Calculations were performed for the undoped and doped cases with no O vacancy present ( $\delta = 0$ ) and one O vacancy present ( $\delta = 0.0625$ ), and the volume change between these two O stoichiometries was determined. This setup was chosen to simplify the calculations, but restricts this study to the mentioned O stoichiometries. For the undoped case (x = 0), these compositions correspond to a range between a stoichiometric to a sub-stoichiometric perovskite. For the doped case (x = 0.125), these compositions span from complete electronic compensation to complete ionic compensation. As a result of this setup, hole states are present in the doped case but not in the undoped case. However, even though not considered here hole states may be possible in undoped perovskites under oxidizing conditions as well. The significance of the hole states will become clearer later in the results section. In addition, although the O stoichiometry in real-world samples likely differ from our calculations (e.g., initial  $\delta > 0$ , final  $\delta < 0.0625$ ), the trends observed and main findings for the simulated compositions are expected to apply.

Although all O sites are equivalent in BaPrO<sub>3</sub> (cubic), they are not equivalent in PrGaO3 (orthorhombic). Since we were more interested in studying trends across varying U values, we simply chose one consistent site for O removal in all PGO/PGM (and BPO/BPY) calculations. Given the large number of possible configurations for distributing the two dopant atoms and one O vacancy, only two extreme cases were considered: (1) dopant atoms and O vacancy close together forming a dopant-vacancy-dopant chain, and (2) dopant atoms and O vacancy distributed far apart. We compared the energies between these two cases, and selected the lower energy case for subsequent analysis. The VESTA program <sup>38</sup> was used to visualize the structures and generate charge density plots. Since BaPrO3 is reported to be antiferromagnetic (AFM) at 0 K<sup>39</sup>, BPO and BPY calculations were carried out with spin-polarization included, and initialized with a G-type AFM ordering. Note that the G-type AFM ordering was only maintained after relaxation by stoichiometric BaPrO3, but became disrupted when defects were introduced. Thus, calculations of BPO (with an O vacancy present) and BPY were repeated a few times slightly varying the initial lattice parameters, which resulted in relaxation to different spin arrangements, and the results were weighted according to a Boltzmann distribution at 900 °C. For the configurations considered, the weighted structures were typically within 1.7 eV of each other for each U value, with differences attributed to electrostatics, strain effects, and magnetism.

The defect formation energy of the O vacancy,  $E^f(v_0)$ , was calculated as

$$E^f(\mathbf{v}_{O}) = E_{tot}(\text{with } \mathbf{v}_{O}) - E_{tot}(\text{without } \mathbf{v}_{O}) + \frac{1}{2}\mu_{O_2}(T, P) , \quad (2)$$

where  $E_{tot}$  (with  $v_O$ ) and  $E_{tot}$  (without  $v_O$ ) are the total energies

of the supercells with and without an O vacancy respectively.  $\mu_{O_2}(T,P)$  is the chemical potential of an oxygen gas molecule at temperature T and pressure P, evaluated by

$$\mu_{O_2}(T, P) = E_{O_2}^{\text{DFT, PBE}} + E_{O_2}^{\text{corr}} + E_{O_2}^{\text{ZPE}} + \Delta\mu_{O_2}^{\circ}(T) + k_B T \ln\left(\frac{P}{P^{\circ}}\right) ,$$
(3)

where  $E_{O_2}^{\mathrm{DFT,\,PBE}}$  is the DFT energy of  $\mathrm{O}_2$  calculated using the PBE functional,  $E_{O_2}^{\mathrm{corr}}$  is the energy correction due to overbinding of the  $\mathrm{O}_2$  molecule when using the PBE functional  $^{40}$ ,  $E_{O_2}^{\mathrm{ZPE}}$  is the zero-point energy of  $\mathrm{O}_2$ ,  $\Delta\mu_{O_2}^{\circ}(T)$  is the change in  $\mathrm{O}_2$  chemical potential from 0 K determined from the NIST database  $^{41}$ ,  $k_B$  is the Boltzmann constant, and  $P^{\circ}$  is the reference pressure of 1 atm. We used  $E_{O_2}^{\mathrm{corr}} + E_{O_2}^{\mathrm{ZPE}} + \Delta\mu_{O_2}^{\circ}(T) + k_BT \ln\left(\frac{P}{P^{\circ}}\right) = -1.504$  eV, correponding to T=1173 K = 900 °C and P=1 atm, to calculate the defect formation energies.

## 2.2 Experimental methods

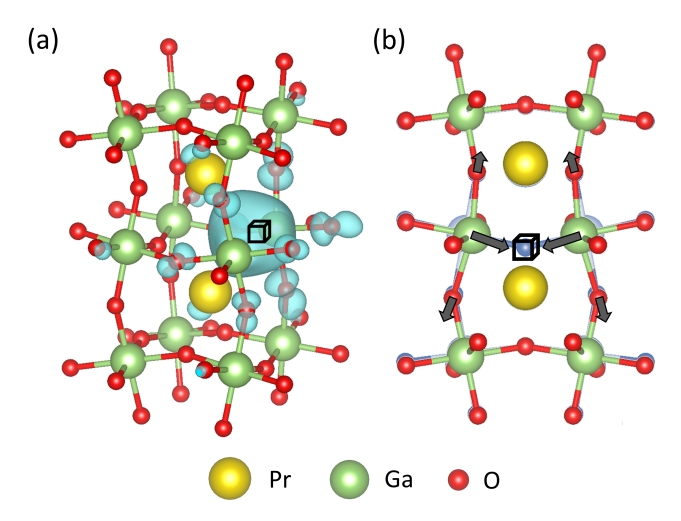
Dense bars of  $PrGa_{0.9}Mg_{0.1}O_{3-\delta}$  and  $BaPr_{0.9}Y_{0.1}O_{3-\delta}$  were synthesized using a modified Pechini method, as described in our prior work  $^{22}$ . The surfaces were ground off using SiC paper immediately prior to conducting the XPS measurements. We performed XPS to assess the average charge states of the nominally multivalent cation, Pr, and to observe the valence band spectra. The latter spectra enable comparison to simulated PDOS for evaluation of appropriate U values. The XPS measurements were carried out using a Kratos Axis ULTRA system (Kratos Analytical), with a monochromatic Al X-ray source and a hybrid spherical capacitor electron energy analyzer detection system. High-resolution scans of the valence band and Pr-3d spectra were taken with a 0.1 eV step size and a 1 second dwell time per step. Scans were analyzed using the CasaXPS version 2.3.25 software  $^{42}$ .

#### 3 Results and discussion

The results and discussion are presented in the following order of materials: (1)  $PrGaO_{3-\delta}$ , (2)  $PrGa_{0.875}Mg_{0.125}O_{3-\delta}$ , (3)  $PrGa_{0.875}Mg_{0.125}O_{3-\delta}$ , (3)  $PrGa_{0.875}Mg_{0.125}O_{3-\delta}$ . For each, we will explain the consequence of O removal as a function of U, and the corresponding impact on the chemical expansion. Subsection (5) presents XPS results to help narrow down U values that better reflect reality. Subsection (6) provides a final summary and discussion of our main findings and plausible explanations for the anomalously low CCEs in PGM and BPY.

#### 3.1 **PrGaO**<sub>3- $\delta$ </sub> ( $\delta = 0 \rightarrow 0.0625$ )

We first present the results for  $PrGaO_{3-\delta}$ , focusing on stoichiometric and sub-stoichiometric compositions. In stoichiometric PGO, Pr exists in the nominal oxidation state of  $Pr^{3+}$ . If Pr is to be reduced during O vacancy formation, this would require the formation of  $Pr^{2+}$ , which is generally a less stable oxidation state <sup>43</sup> than  $Pr^{3+}$ . Indeed, for any value of U, we found that the electrons left behind by a removed oxygen do not reduce the  $Pr^{3+}$  ions, but instead localize predominantly at the O vacancy site forming an F'-center  $(v_0^{\times})$ , as shown by the charge density plot of the defect



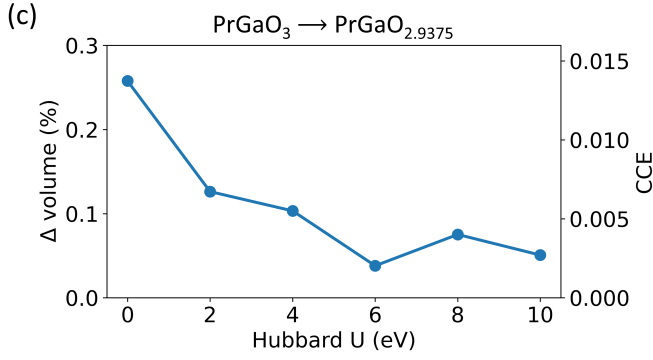


**Fig. 2** (a) Charge density plot of the F'-center formed when an O vacancy (represented by the black box) is introduced to  $PrGaO_3$ , the charge density isosurface is shown in cyan. (b) Relaxation of the lattice ions around the O vacancy, showing Ga ions attracted to the F'-center, and O ions repelled from the F'-center. (c) Percentage volume change as a function of Hubbard U when one O vacancy is introduced to  $PrGaO_3$ . The secondary axis represents the CCE corresponding to each percentage volume change.

state in Fig. 2a. The lattice relaxation around the F'-center is shown in Fig. 2b, where the neighboring  $Ga^{3+}$  ions have moved closer to the O vacancy, whereas the nearest neighbor  $O^{2-}$  ions have moved away from the O vacancy, as a result of the interaction with the localized electrons. We found the net effect of all atomic displacements to result in a small lattice expansion. In the alternative case where oxygen vacancies form with no localized electrons ( $v_0^{\bullet\bullet}$ ), the two electrons usually localize at and reduce cations. In this case, the lattice ions around the vacancy usually displace in the opposite directions to those observed here for the F'-center, and are most commonly associated with lattice contraction  $^{17,44,45}$  (if the cation radius increase due to reduction is ignored).

Hence, despite the lack of reduced cations, formation of an F'-center still causes chemical expansion in PGO, albeit smaller than usual. For reference, the redox CCE of typical perovskite materials falls in the range of 0.02–0.06<sup>4</sup>. Fig. 2c shows the percentage volume change of PGO as a function of U, and the corresponding CCEs are indicated on the secondary axis. Since the CCEs are calculated over a large  $\Delta\delta$ , they should be interpreted as the average

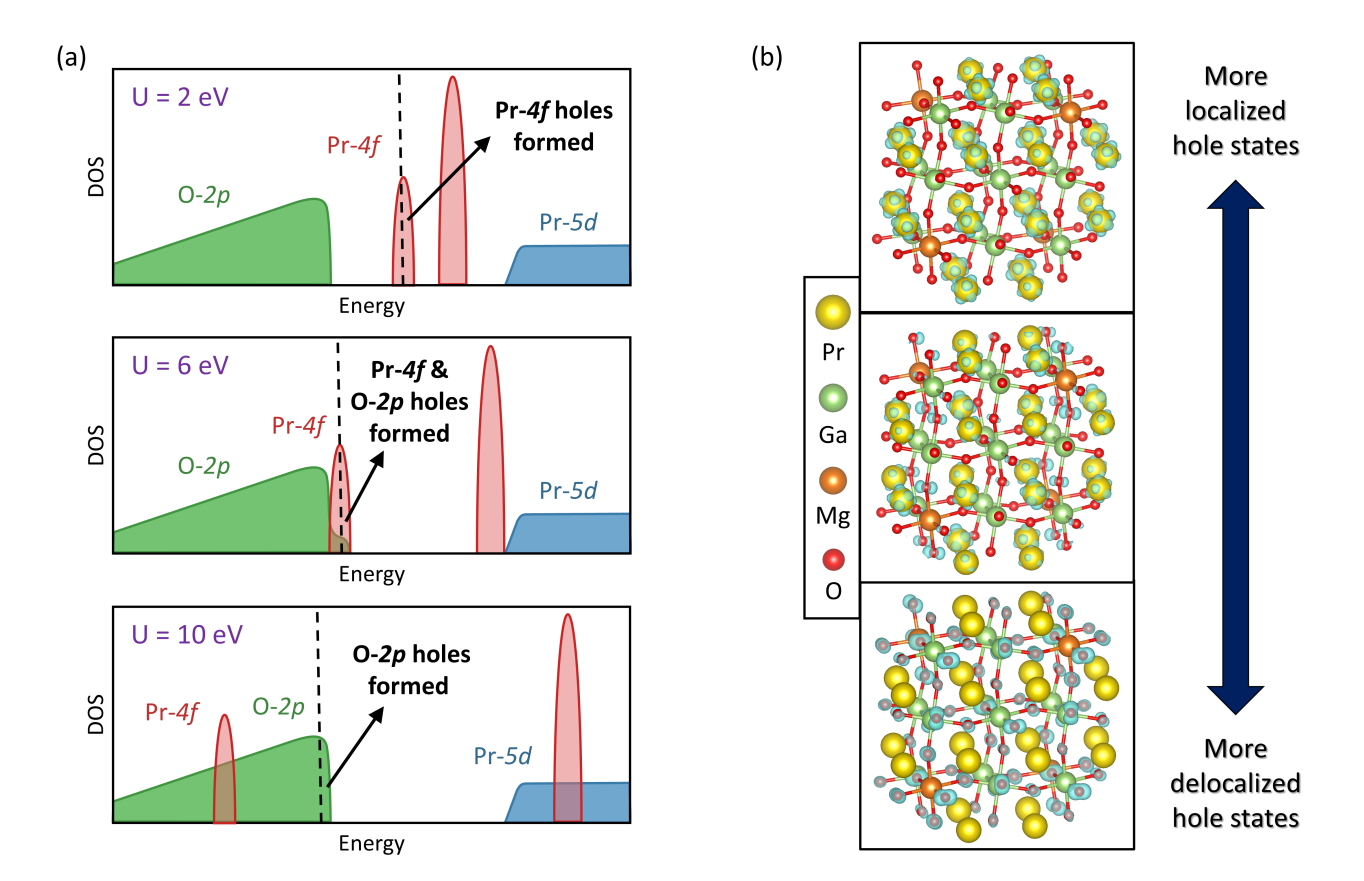


Fig. 3 (a) Simplified depiction of the PDOS of  $PrGa_{0.875}Mg_{0.125}O_3$  showing the different hole states formed at U=2, 6, and 10 eV. The black dashed line represents the Fermi level. See ESI Fig. S2 for actual PDOS. (b) The corresponding partial charge density plots of the hole states at U=2, 6, and 10 eV. The charge density isosurface is shown in cyan.

CCE over the  $\Delta\delta$  range. As the parameter U increases from left to right, the percentage volume change initially decreases, indicating that the lattice expansion becomes even smaller with higher localization of the Pr-4f electrons. The larger expansion observed for small  $U\approx 0$  eV arises because the occupied and unoccupied Pr-4f states shown in Fig. 1c are not isolated, but form a single band of partially occupied states. The splitting of the occupied and unoccupied Pr-4f states when U>0 eV results in a sudden increase in the localization of the 4f valence electrons around Pr. Here we see an example of electron localization causing smaller lattice expansions instead of the opposite, in contrast to the previously mentioned case of  ${\rm CeO}_{2-\delta}$ . For U>4 eV, the percent expansion drops below 0.1%. The small fluctuations beyond U>4 eV are likely due to numerical noise, since the degree of expansion is small to begin with.

#### 3.2 $PrGa_{0.875}Mg_{0.125}O_{3-\delta}$ ( $\delta = 0 \rightarrow 0.0625$ )

We now move on to  $PrGa_{0.875}Mg_{0.125}O_{3-\delta}$ , for which the composition is associated with hole states in contrast to the prior PGO analysis. We studied the case where PGM is fully electronically compensated initially, and subsequently becomes fully ionically compensated by O removal. The results shown are with respect to the arrangement of Mg and O vacancy far apart, which

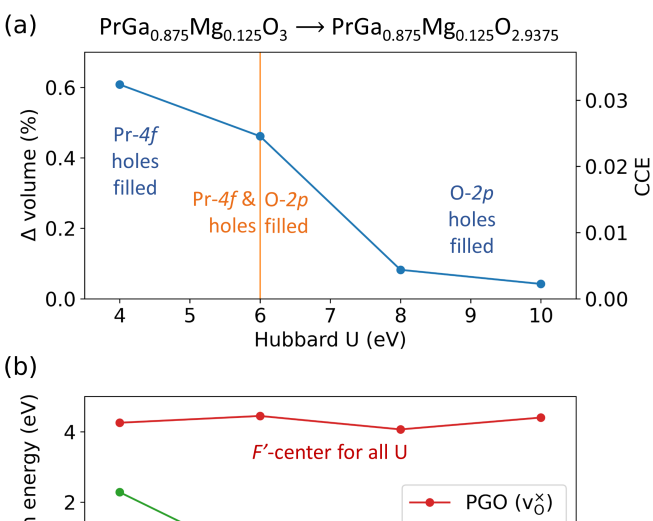
we found to be more energetically favorable† than the close together arrangement by at least 0.17 eV per pair of Mg dopants. When  $\delta = 0$ , the introduction of Mg acceptors to PrGaO<sub>3</sub> results in holes that form to maintain electroneutrality, where the natural expectation is for holes to appear in the form of Pr<sup>4+</sup>. Perhaps non-intuitively, the nature of holes formed is more complex, showing a dependence on the degree of localization of the Pr-4f electrons as illustrated from the PDOS shown in Fig. 3a. Depending on the value of parameter U, the holes may be located on Pr, Pr-O hybridized<sup>‡</sup> states, or even on O. The formation of  $Pr^{4+}$  ([Xe]  $4f^1$ ) requires the removal of one 4f electron from  $Pr^{3+}$  ([Xe]  $4f^2$ ). When U < 6 eV, the highest occupied orbital of PrGaO<sub>3</sub> consists of Pr-4f states, and the Pr-4f electrons are simply removed to form Pr hole states (Pr<sup>4+</sup>) in PrGa<sub>0.875</sub>Mg<sub>0.125</sub>O<sub>3</sub>. However, when U is increased to 6 eV, the Pr-4f states in the valence band are shifted far enough to the left that they overlap with O-2p states, such that the valence band maximum (VBM)

<sup>‡</sup> Although we refer to hybridization by its common usage to denote the covalent sharing of electron density between different atoms, we note that hybridization technically refers to the combination of orbitals within the same atom <sup>46</sup>.

now consists of both Pr-4f and O-2p states. As a result, Mg doping creates Pr-4f/O-2p hybridized hole states. Further increasing U beyond 6 eV causes the Pr-4f states to drop below the O-2p states, interestingly resulting in only O-2p hole states being formed in PrGa<sub>0.875</sub>Mg<sub>0.125</sub>O<sub>3</sub>. As such, if the Pr-4f electrons are sufficiently localized, O-2p holes can actually form in PGM, despite Pr being present as a nominally multivalent ion.

The nature of the holes has a significant consequence on the chemical expansion, as it is these hole states that will typically be filled by the electrons left behind when an oxygen vacancy forms. In particular, we highlight the difference in the degree of delocalization of the hole states, which is distinct from the degree of delocalization of the Pr-4f electrons. Fig. 3b shows the charge density of hole states corresponding to each PDOS shown in Fig. 3a. When U = 2 eV, Pr-4f hole states form and they are seen to spread throughout all Pr ions. When U = 6 eV, O-2p hole states begin to form on some O ions along with the Pr-4f hole states, creating more delocalized hole states. When U = 10 eV, only O-2p hole states form and they spread throughout all O ions, creating even more delocalized hole states. These hole states are essentially the same as O valence band states and are maximally delocalized. Therefore, as the Pr-4f states become more localized, the hole states formed by Mg doping instead become more delocalized, and the electrons left behind during oxygen vacancy formation fill these more delocalized states. This behavior is the opposite of the behavior reported <sup>18</sup> for  $CeO_{2-\delta}$  and  $BaCeO_{3-\delta}$ . In those cases it was found that the more localized the Ce-4f states, the more localized the states filled during oxygen vacancy formation. The reason for the different behavior is that hole states are present here initially such that excess electrons compensate the hole states. In the previous computational studies, hole states were not considered so excess electrons instead reduced the multivalent cations.

The filling of more delocalized states is expected to cause smaller chemical expansions, and indeed this is the result that we found. Fig. 4a<sup>†</sup> shows the volume change and CCE as a function of U when one O vacancy is introduced to  $PrGa_{0.875}Mg_{0.125}O_3$ . As PGM transitions from filling Pr-4f hole states to filling O-2p hole states, a sharp drop in volume change is observed corresponding to the increase in delocalization of the hole states. Whilst the filling of Pr-4f holes leads to CCEs that are on par with typical perovskite materials, the filling of O-2p holes leads to CCEs that are an order of magnitude smaller, a feature that would be highly desirable for minimizing the mechanical degradation of devices. The defect formation energy of  $\mathbf{v}_{\mathbf{O}}^{\times}/\mathbf{v}_{\mathbf{O}}^{\bullet\bullet}$  as a function of U for both PGO and PGM is shown in Fig. 4b. The formation of an F'-center  $(v_O^{\times})$  in PGO has a high formation energy that is virtually independent of U. On the other hand, the  $v_0^{\bullet \bullet}$  formation energy in PGM decreases as U increases, since the VBM where hole states



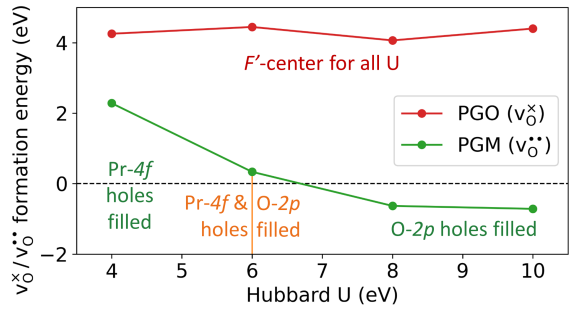


**Fig. 4** (a) Percentage volume change as a function of Hubbard U for introducing one O vacancy to  $PrGa_{0.875}Mg_{0.125}O_3$ . The secondary axis represents the CCE corresponding to each percentage volume change. (b) Defect formation energy of 1 O vacancy in  $PrGaO_3$  and  $PrGa_{0.875}Mg_{0.125}O_3$  as a function of Hubbard U. The Mg dopant atoms and O vacancy are arranged far apart for the results shown.

are located shifts down in energy with increasing U (refer to Fig. 3a), until it is eventually fixed near the top of the O-2p states at sufficiently high U. Hence, the formation of O vacancies in PGM becomes more favorable with increasing localization of the Pr-4f electrons.

#### 3.3 BaPrO<sub>3- $\delta$ </sub> ( $\delta = 0 \rightarrow 0.0625$ )

Next, we present the results for BaPrO<sub>3- $\delta$ </sub>. Similar to PGO, we start from the stoichiometric perovskite and remove one oxygen atom from the supercell. One major difference of having Pr on the B-site instead of the A-site of the perovskite is that BaPrO<sub>3</sub> demonstrates prominent hybridization of the Pr-4f and O-2p states <sup>47–49</sup>, resulting in higher bond covalency. As such, the nominal valence state of Pr<sup>4+</sup> based on the assumption of fully ionic bonding is no longer appropriate. Instead, Pr is reported to exist in mixed-valence states of  $Pr^{3+}$  ([Xe]  $4f^2$ ) and  $Pr^{4+}$  ([Xe]  $4f^1$ ) in BaPrO<sub>3</sub> <sup>49</sup>. Our DFT calculations also show significant Pr-4f/O-2p hybridization in BaPrO<sub>3</sub> (refer to Fig. S13 of Ref. 22), where the covalency of the Pr–O bond depends on the value of U. The average Pr-4f occupancy was calculated by integrating the Pr-4f density of states in the valence band, and is shown as a function of U in Fig. 5a. For low U values, the 4f occupancy is close to 2 and the valence state can be described as  $Pr^{3+}$ . As U increases and the Pr-4f electrons become more localized, there is less overlap between the Pr-4f and O-2p orbitals, resulting in less Pr-4f/O-2p hybridization. Thus, the 4f occupancy decreases and the Pr-O

 $<sup>\</sup>dagger$  For U<4 eV, the electrons left behind by the removed oxygen did not fill the Pr-4f hole states, but instead formed an F'-center similar to PGO. This anomaly is due to the low degree of localization of the Pr-4f electrons (low U value), resulting in the F'-center defect state being lower in energy than the Pr-4f hole states (refer to ESI Fig. S2), and thus more favorable to form than filled Pr-4f hole states. The results for U<4 eV are therefore not shown in Fig. 4.

bond is more ionic. Conventionally, it is common to describe Pr as being in mixed  $\Pr^{3+}([Xe]\ 4f^2)$  and  $\Pr^{4+}([Xe]\ 4f^1)$  valence states, but a more accurate description is that each Pr ion has one electron occupying a  $\Pr^{4}f$  orbital and further shares electrons with O through hybridized  $\Pr^{4}f/O^{2}p$  orbitals.

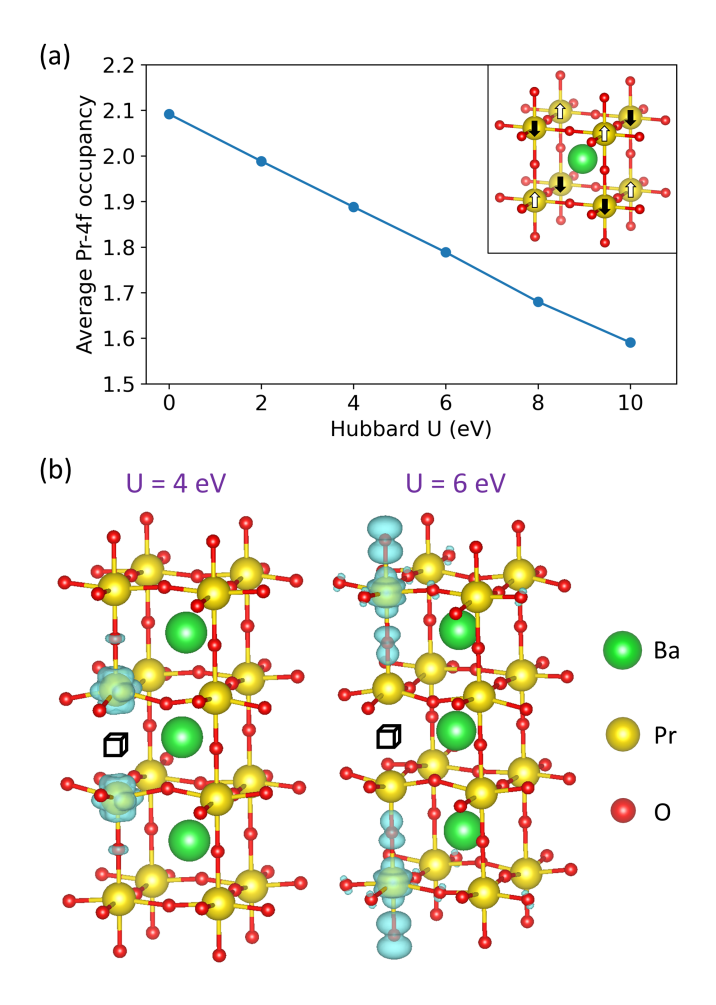


**Fig. 5** (a) Average Pr-4f occupancies of stoichiometric BaPrO<sub>3</sub> as a function of Hubbard U. The inset shows the antiferromagnetic ordering of stoichiometric BaPrO<sub>3</sub>, where the Pr spin directions are indicated by the arrows. (b) Partial charge density plots of Pr-4f states (U=4 eV) or hybridized Pr-4f/O-2p states (U=6 eV) filled by the electrons left behind when an O vacancy is introduced to BaPrO<sub>3</sub>.

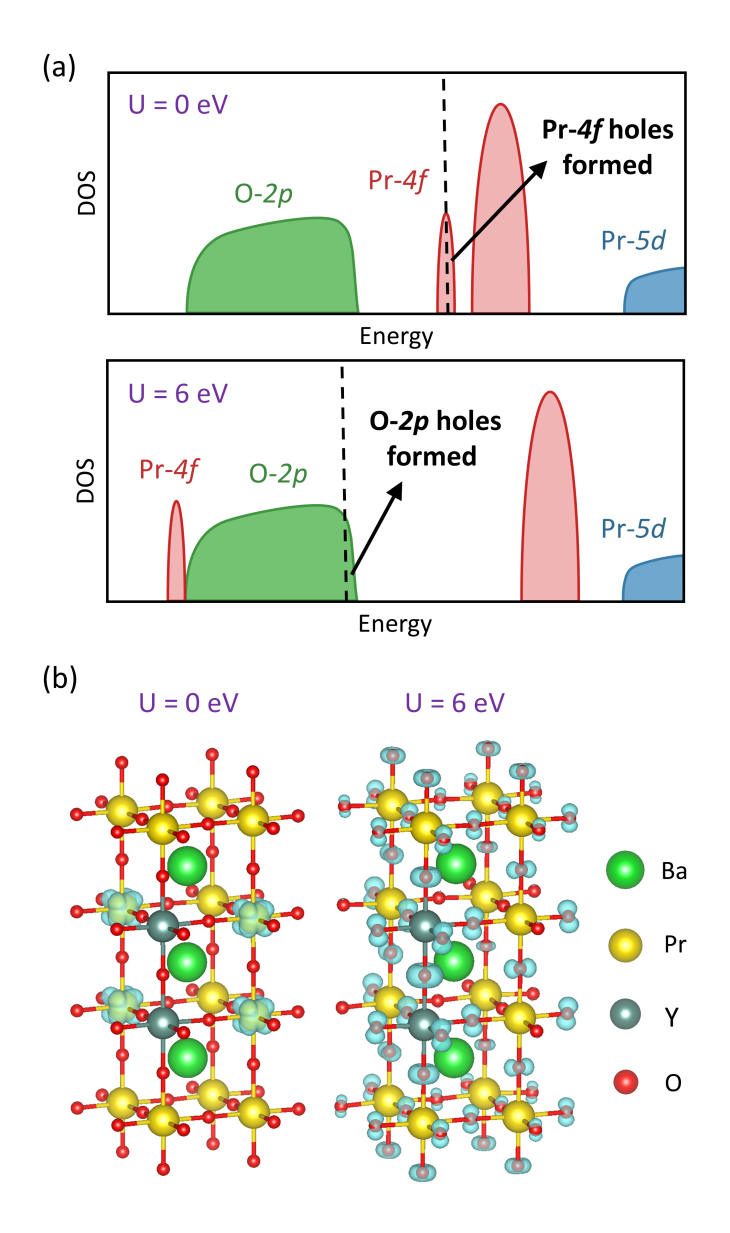
An O vacancy was then introduced to BaPrO<sub>3</sub>, just as we did for PrGaO<sub>3</sub>. We found that the antiferromagnetism of BPO coupled with O vacancy formation made the calculations numerically challenging, and we were able to obtain physical and well-converged results only for U=4 and 6 eV, which are highlighted here. For U<4 eV, the challenge came from the implied reduction of  $\Pr^{3+}$  to  $\Pr^{2+}$ ; for higher values of U>6 eV, the challenge came from excessively localized  $\Pr^{4}$  states. However, for U=4 and 6 eV, the removal of one O resulted in electrons filling states as shown in Fig. 5b. Distinct from the case of PGO shown previously, we find that here the electrons introduced by the oxygen vacancy now do reduce the multivalent  $\Pr$  cations. This behavior is more in line with what has been reported for other oxide materials, and correspondingly the reduction of  $\Pr$  is associated with a large

volume expansion (CCE): 0.729% (0.039) and 1.18% (0.063) for U = 4 and 6 eV respectively. The main reason for the difference is because the Pr ions in BPO (average valency between 3+ and 4+) can be reduced to Pr<sup>3+</sup>, whereas the Pr<sup>3+</sup> ions in PGO cannot be reduced to Pr<sup>2+</sup>. As Fig. 5b shows, the electrons distribute in different ways (i.e., to the Pr around the vacancy for U = 4 eV and to the Pr–O network for U=6), and generally we observe that the electrons may distribute across BPO in other ways depending on the final magnetic ordering. Overall, however, the formation of an O vacancy in BPO leads to the reduction of Pr as would be intuitively expected. The defect formation energies of  $v_0^{\bullet\bullet}$  are 1.95 eV and 2.06 eV for U=4 and 6 eV respectively. The  $v_{O}^{\bullet \bullet}$  formation energy does not appear to change much with U, since the introduction of an O vacancy creates mid-gap defect states in BPO (refer to ESI Fig. S3), instead of filling hole states that can shift in energy with U like in PGM.

#### 3.4 BaPr<sub>0.875</sub>Y<sub>0.125</sub>O<sub>3- $\delta$ </sub> ( $\delta = 0 \rightarrow 0.0625$ )

We now turn to the case where hole states are considered, BaPr<sub>0.875</sub> $Y_{0.125}O_{3-\delta}$ . Just like PGM, we considered compositions ranging from complete electronic compensation to complete ionic compensation. BPY interestingly behaves similarly to PGM (despite the differences observed between parent compounds BPO and PGO). Here the results are shown with respect to the arrangement of Y dopants and O vacancy close together, which was found to be more energetically favorable than the far apart arrangement by at least 0.14 eV per pair of Y dopants. Also, for BPY we were able to obtain physical and well-converged results for smaller U < 4 eV, unlike the case for BPO. Fig. 6a shows a schematic of the PDOS of BaPr<sub>0.875</sub>Y<sub>0.125</sub>O<sub>3</sub>, where the type of holes formed with acceptor doping is again dependent on the value of U. When U is below approximately 2 eV, Pr-4f hole states are formed. When U is approximately 2 eV, the Pr-4f states in the valence band begin to overlap with the O-2p states, so Pr-4f/O-2p hybridized hole states are formed. When U is above approximately 2 eV, O-2p hole states are formed. The O-2p hole states are again more delocalized than the Pr-4f hole states, as shown in Fig. 6b. The O-2p hole states are distributed across all O ions, whereas the Pr-4f hole states are located on four Pr ions neighboring the Y dopants. By comparing Figs. 3b and 6b for the lower values of U, it is interesting to note that the Pr-4f hole states are more localized in BPY compared to PGM. Both PGM and BPY are doped on the B-site, and placement of Pr on the Bsite in BPY likely allowed for more localized hole states to form next to the dopant atoms.

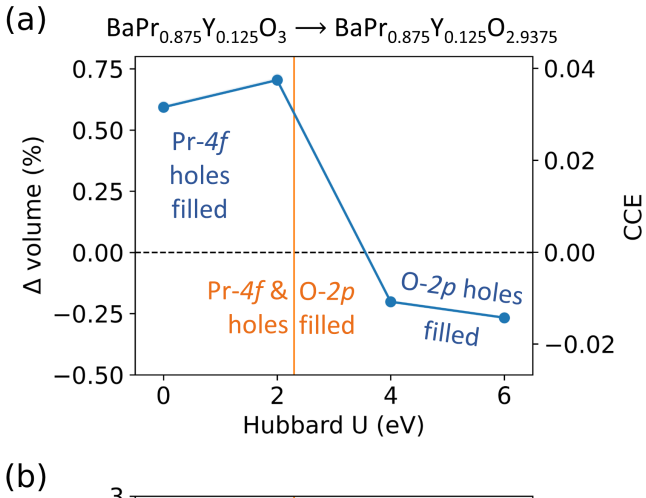
The filling of the more delocalized O-2p hole states during O removal similarly leads to smaller volume changes than the filling of the more localized Pr-4f hole states, as shown in Fig. 7a. Volume changes of  $\approx$  0.6-0.7 % (CCE  $\approx$  0.03-0.04) are observed for small values of U, which quickly reduce as U further increases. In fact, negative volume changes (lattice contractions) are obtained when O-2p hole states are filled. This occurs as a result of the close arrangement of the Y dopants and O vacancy, where a similar behavior is found for PGM when the Mg dopants and O vacancy are arranged close together instead of far apart (i.e., the plot in



**Fig. 6** (a) Simplified depiction of the PDOS of BaPr $_{0.875}$ Y $_{0.125}$ O $_{3}$ , where the black dashed line represents the Fermi level. Pr-4f holes are formed at U=0 eV, and O-2p holes are formed at U=6 eV. See ESI Fig. S4 for actual PDOS. (b) Partial charge density of the holes formed due to Y doping, the charge density isosurface is shown in cyan. Adapted with permission from Ref. 22. Copyright 2021 American Chemical Society.

Fig. 4a would shift downwards). If we apply the framework of treating chemical expansion as a competition between (1) lattice expansion due to the reduction of cations and (2) lattice contraction around the O vacancy due to electrostatic effects, then a net lattice contraction occurs when the latter outweighs the former. In this case, assuming that the lattice expansion due to the reduction of ions is similar across different arrangements of dopant atoms and O vacancies<sup>†</sup>, then the lattice contraction around the O vacancy appears to be larger when the dopant atoms and O va-

cancies are arranged close together than when they are far apart. Nonetheless, the trend remains the same where a sharp drop in volume change occurs when BPY transitions from filling Pr-4f hole states to filling O-2p hole states. The defect formation energy of  $\mathbf{v}_{\mathbf{0}}^{\bullet\bullet}$  in BPY is shown in Fig. 7b as a function of U. Similar to PGM, the  $\mathbf{v}_{\mathbf{0}}^{\bullet\bullet}$  formation energy decreases as U increases since the hole states being filled become shifted to lower energies.



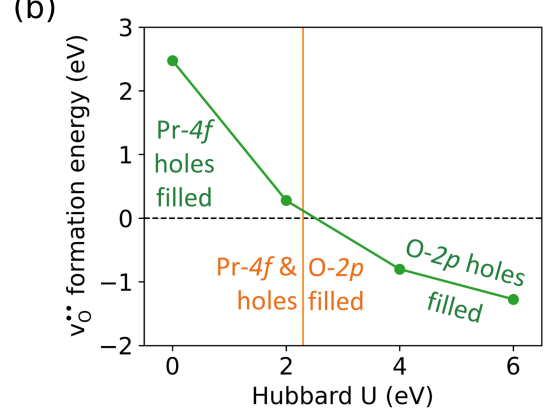


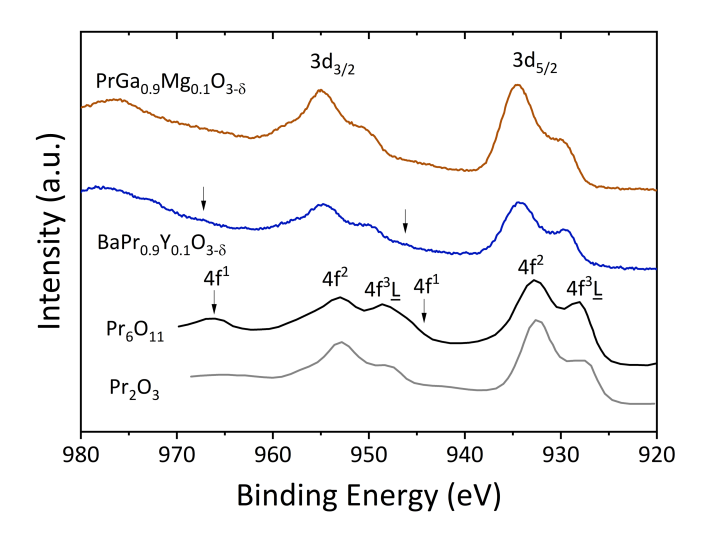
**Fig. 7** (a) Percentage volume change as a function of Hubbard U for introducing one O vacancy to  $\mathsf{BaPr}_{0.875}\mathsf{Y}_{0.125}\mathsf{O}_3$ . The secondary axis represents the CCE corresponding to each percentage volume change. (b) Defect formation energy of 1 O vacancy in  $\mathsf{BaPr}_{0.875}\mathsf{Y}_{0.125}\mathsf{O}_3$  as a function of Hubbard U. The Y dopant atoms and O vacancy are arranged close together for the results shown.

#### 3.5 XPS of PGM and BPY

Considering the significant difference in CCE depending on whether Pr-4f or O-2p hole states are formed, we performed XPS measurements of PGM and BPY to characterize their actual electronic structures, help determine if O holes contribute to their near-zero CCEs  $^{22}$ , and identify the range of the parameter U that more realistically describes each material. Note that the dopant concentration is slightly different in the experiments (10 %) compared to the computational calculations (12.5 %). Fig. 8 shows the Pr-3d spectra of PGM and BPY compared to other reference Pr oxides. The valence state of Pr is 3+ in  $Pr_2O_3$ , whereas it is mixed 3+ and 4+ in  $Pr_6O_{11}$   $^{50}$ . The presence of  $Pr^{4+}$  in  $Pr_6O_{11}$ 

 $<sup>\</sup>dagger$  We find that the degree of localization of the hole states does not change significantly between arrangements of dopant atoms and O vacancy close together or far apart for a given U value.

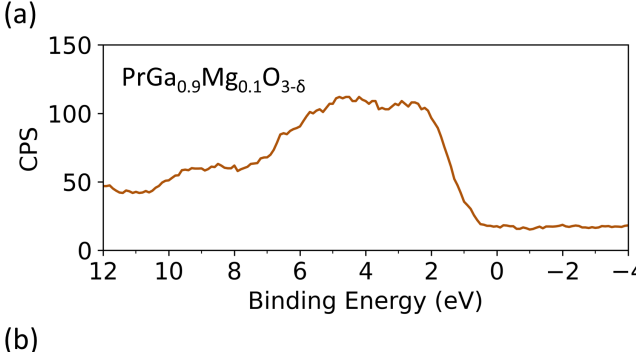
is evidenced by a peak corresponding to the  $4f^1$  state at ~966 eV and its doublet peak at ~945 eV<sup>51</sup>. Pr<sub>6</sub>O<sub>11</sub> also exhibits a higher relative intensity of the low energy shoulder,  $4f^3\underline{L}$ , at both the  $3d_{5/2}$  and  $3d_{3/2}$  doublet peaks. These  $4f^3\underline{L}$  peaks (where  $\underline{L}$  indicates a hole on oxygen) have been attributed to strong covalent mixing between Pr and O ions<sup>51,52</sup>.



**Fig. 8** Pr-3d spectra of PrGa $_{0.9}$ Mg $_{0.1}$ O $_{3-\delta}$  and BaPr $_{0.9}$ Y $_{0.1}$ O $_{3-\delta}$  samples. Reference spectra for Pr $_6$ O $_{11}$  and Pr $_2$ O $_3$  are taken from Ref. 51. The arrows indicate the positions of  $4f^1$  peaks.

Determination of quantitative Pr<sup>3+</sup>/Pr<sup>4+</sup> ratios from the XPS data requires fitting; however, the multiple strategies reported in the literature for this purpose 52-54 return different results (see ESI Supplementary Note 1 for further details). Therefore, we restrict our analysis to only a qualitative comparison between our materials and the reference oxides as follows: Compared to Pr<sub>2</sub>O<sub>3</sub> and  $Pr_6O_{11}$ , the main  $3d_{5/2}$  and  $3d_{3/2}$  peaks are shifted to higher energies in PGM and BPY, consistent with the observations in other mixed Pr oxides 53. The lack of discernable  $4f^1$  peaks in PGM indicates that there is little to no Pr<sup>4+</sup> present, even though < 10 % Pr<sup>4+</sup> (accounting for O vacancies present in the sample) is expected for PGM if Pr holes form. This suggests the possibility of PGM being compensated by O holes instead of Pr holes, which could explain its anomalously small CCE  $^{22}$ . For BPY,  $4f^1$  peaks can be observed at 967.5 eV and 946.0 eV, but their intensities are very low. This indicates a low concentration of Pr<sup>4+</sup> in BPY, consistent with the significant Pr-O bond covalency mentioned previously, which gives an effective valence state lower than 4+. The bond covalency is also supported by the higher relative intensity of the  $4f^3\underline{L}$  peaks for BPY compared to PGM. The low Pr<sup>4+</sup> concentration may also be contributed by oxygen deficiency in the sample, or the formation of O holes instead of Pr holes.

The valence band XPS spectra are shown in Fig. 9, which can be compared to the PDOS in Fig. S2 and S4 (see ESI Supplementary Note 2 for discussion on discrepancies). We do not observe an isolated (Pr-4f) peak located to the right of the broad (O-2p) feature at the top of the valence band, indicating that the Pr-4f peak is joined with O-2p states. However, these spectra are not element-specific, so the relative positions of the Pr and O states



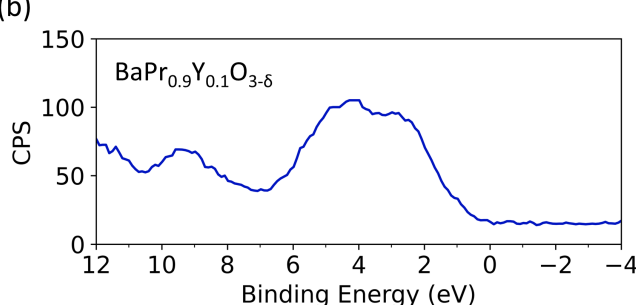


**Fig. 9** Valence band XPS spectra of (a)  $PrGa_{0.9}Mg_{0.1}O_{3-\delta}$  and (b)  $BaPr_{0.9}Y_{0.1}O_{3-\delta}$ . CPS stands for counts per second.

cannot be determined unambiguously here, making it indeterminate if the top of the valence band consists of O states, Pr states, or both.

Although our XPS results cannot fully confirm the presence of O holes, they do support the possibility, and show that the Pr-4fpeak in the valence band does not exist as an isolated peak to the right of the O-2p states. Furthermore, photoelectron spectroscopy (PES) data of BaPrO<sub>3</sub> from literature 55,56 reported Pr states to be located near the top of the O states in the valence band. PrInO<sub>3</sub> <sup>57</sup>, which shares the same crystal structure as PrGaO<sub>3</sub>, was also reported to have Pr states located near the top of the O-2p states. Ultimately, these findings suggest that U values in the range of 6-8 eV and 2-4 eV would be appropriate for PGO/PGM and BPO/BPY respectively. A comparison to calculations employing the Heyd-Scuseria-Ernzerhof (HSE06) hybrid functional <sup>58</sup> is provided in the ESI (see Fig. S6). The PDOS calculated using HSE06 closely match those calculated using PBE and U = 4 eV throughout most of the domain, showing that HSE06 can provide a reasonable description of BPO/BPY (albeit at much higher computational cost), but not of PGO/PGM.

#### 3.6 Main findings and insights

The relationship between electron localization and chemical expansion shows a complex and sometimes non-intuitive dependence on the nature of the states filled by the electrons left behind by removed oxygen atoms. The most intuitive case is when the multivalent cation is reduced, such as in  $\text{CeO}_{2-\delta}$ , where localization of the Ce-4f electrons results in larger chemical expansions. We observe this behavior for BPO, which shows chemical expansion similar in magnitude to those reported for other perovskite materials. For BPO, however, the degree of metal-oxygen

hybridization is sensitive to the degree of electron localization, as probed by varying the parameter U. As the Pr-4f electrons become more localized, the Pr-4f/O-2p orbitals become less hybridized, and the degree to which Pr can be reduced increases (i.e., Pr reduces over a larger range of  $\Delta\delta$ ). On the other hand, if the reduction of the multivalent cation does not occur as found for PGO in the range of O stoichiometry we studied, then F'-centers may form. The degree of chemical expansion is smaller in this case, and becomes even smaller as the Pr-4f electrons became more localized.

When a material has hole states present, the hole states now determine the chemical expansion behavior, since they are the states that become filled during O vacancy formation. This link between the nature of hole states and the degree of chemical expansion presents a new perspective from which to view the relationship between electron localization and chemical expansion, since the nature of the hole states can change with electron localization as we have shown. It is now the degree of localization of the hole states that directly influences the magnitude of the chemical expansion, rather than the degree of localization of the metal cation electrons. In fact, as shown for PGM and BPY, localization of the Pr-4f electrons instead led to the delocalization of the hole states. We highlight that the formation of more delocalized O hole states compared to metal hole states can potentially allow for a significant decrease in CCE of a material. However, note that decreasing the multivalent cation concentration (e.g., Ni in LSGN or Fe in STF) will only localize the multivalent cation electrons by spacing the multivalent cations atoms further apart, but will unlikely change the type of hole states formed (i.e., will unlikely form O holes). Also, note that even if a perovskite is not acceptor-doped, hole states may still form under oxidizing conditions.

In the case that the hole states are located on the multivalent ion, they may become more delocalized if the multivalent ion is placed on the A-site instead of the B-site, as we have seen for the case of PGM vs. BPY for lower U values. Additionally, the empirical model for the perovskite lattice parameter developed by Marrocchelli et al. 17 predicts a smaller CCE for the same increase in ionic radius at the A-site compared to the B-site. Indeed, for the lower U values where only Pr-4f holes form, we do find that the % volume expansion of PGM is around half of that of BPY for similar arrangements of the dopant atoms and O vacancy. Therefore, as we discussed in our earlier work <sup>22</sup>, placing the multivalent cation on the A-site would likely lower the CCE appreciably when designing perovskite materials with multivalent cations. However, if the holes are instead located on oxygen or hybridized cation-oxygen orbitals, then the CCE would likely be similar regardless of A-site/B-site placement. The anisotropic expansion of orthorhombic PGM (see ESI Fig. S7) may have also contributed to its lower volume expansion compared to cubic BPY when Pr-4f holes are filled. A contraction along the b-axis is observed for all values of U, and is also found in our experimental measurements <sup>22</sup>. Lower symmetry phases which can expand anisotropically have been reported to expand less, macroscopically, than their symmetric counterparts <sup>7,20</sup>.

Finally, our hypothesis of O hole filling is consistent with the ex-

perimental observations reported for PGM and BPY  $^{22}$ . Their CCEs are both anomalously small regardless of A-site/B-site placement of Pr, which would be unusual if Pr is being reduced. Conductivity measurements revealed relatively low activation energies for electronic conduction, which is consistent if delocalized O holes are present. XPS results showed little to no  $Pr^{4+}$  present, suggesting the lack of Pr holes. In spite of this corroborating evidence, we emphasize that it is not possible to unambiguously attribute the low CCEs to O-2p holes. For instance, some hole states may have been eliminated by existing O vacancies in the samples. The bond covalency of BPY also leads to a naturally lower concentration of  $Pr^{4+}$  than if the bonding is fully ionic, complicating the analysis. Nonetheless, our hypothesized mechanism remains in agreement with experimental observations and appears to be viable given the computational and experimental results presented here.

## 4 Conclusions

The degree of electron localization can significantly affect the chemical expansion of oxide materials, providing a potential route to modify their CCEs based on the needs of their applications. In this work, we have studied the chemical expansion of PGO, PGM, BPO, and BPY, under varying degrees of localization of the Pr-4f electrons through DFT+U calculations, and also carried out XPS characterization. Whilst some materials may exhibit a simple relationship of increased chemical expansion with increased electron localization, we showed that the relationship is not as straightforward for the Pr-based perovskite materials investigated here, as Pr is not necessarily reduced with the removal of oxygen. We showed the formation of an F'-center in PGO due to the unfavorable reduction of Pr3+, and Pr reduction in BPO that is dependent on the covalency of the Pr-O bond. The relationship between electron localization and chemical expansion depends on the chemistry of the material, and in the case of materials with hole states present, special attention needs to be given to the nature of the hole states. Both PGM and BPY showed the formation of Pr-4f hole states at lower U values, which changed to the formation of O-2p hole states at higher U values. The O-2p hole states were more delocalized than the Pr-4f hole states, resulting in far smaller volume expansions than typical perovskites when the O-2p hole states were filled during O removal. We highlight the non-intuitive behavior of changing hole types with electron localization, and the possibility of engineering materials with ultra-low CCEs through the formation of oxygen holes.

#### Conflicts of interest

There are no conflicts to declare.

#### Acknowledgements

This work was supported by funding from NSF grant no. 1545907 through a JSPS-NSF Partnership for International Research and Education (PIRE), NSF CAREER grant no. DMR-1945482 awarded to NHP, and U.S. Army CERL W9132T-19-2-0008. Calculations were performed on the Illinois Campus Cluster, operated by the Illinois Campus Cluster Program (ICCP) in conjunction with the National Center for Supercomputing Applications (NCSA) and supported by funds from the University of

Illinois at Urbana-Champaign. XPS measurements were carried out by Richard T. Haasch in the Materials Research Laboratory Central Research Facilities, University of Illinois.

#### References

- 1 S. R. Bishop, Acta Mechanica Sinica, 2013, **29**, 312–317.
- 2 P. N. Dyer, R. E. Richards, S. L. Russek and D. M. Taylor, <u>Solid</u> State Ionics, 2000, **134**, 21–33.
- 3 S. B. Adler, <u>Journal of the American Ceramic Society</u>, 2001, 84, 2117–2119.
- 4 S. Bishop, D. Marrocchelli, C. Chatzichristodoulou, N. Perry, M. Mogensen, H. Tuller and E. Wachsman, <u>Annual Review of Materials Research</u>, 2014, **44**, 205–239.
- 5 N. H. Perry, J. J. Kim, S. R. Bishop and H. L. Tuller, <u>Journal of</u> Materials Chemistry A, 2015, **3**, 3602–3611.
- 6 K. L. Duncan, Y. Wang, S. R. Bishop, F. Ebrahimi and E. D. Wachsman, <u>Journal of the American Ceramic Society</u>, 2006, **89**, 3162–3166.
- 7 V. V. Kharton, A. V. Kovalevsky, M. Avdeev, E. V. Tsipis, M. V. Patrakeev, A. A. Yaremchenko, E. N. Naumovich and J. R. Frade, Chemistry of Materials, 2007, **19**, 2027–2033.
- 8 S. M. Selbach, A. Nordli Løvik, K. Bergum, J. R. Tolchard, M.-A. Einarsrud and T. Grande, <u>Journal of Solid State Chemistry</u>, 2012, **196**, 528–535.
- 9 W. H. Woodford, W. C. Carter and Y.-M. Chiang, <u>Energy</u> Environmental Science, 2012, **5**, 8014–8024.
- 10 K. Sato, H. Omura, T. Hashida, K. Yashiro, H. Yugami, T. Kawada and J. Mizusaki, <u>Journal of Testing and Evaluation</u>, 2006, **34**, 246–250.
- 11 K. Sato, K. Yashiro, T. Kawada, H. Yugami, T. Hashida and J. Mizusaki, <u>Journal of Power Sources</u>, 2010, **195**, 5481–5486.
- 12 J. G. Swallow, J. J. Kim, J. M. Maloney, D. Chen, J. F. Smith, S. R. Bishop, H. L. Tuller and K. J. Van Vliet, <u>Nature Materials</u>, 2017, **16**, 749–754.
- 13 Y.-M. Kim, J. He, M. D. Biegalski, H. Ambaye, V. Lauter, H. M. Christen, S. T. Pantelides, S. J. Pennycook, S. V. Kalinin and A. Y. Borisevich, <u>Nature Materials</u>, 2012, 11, 888–894.
- 14 S. R. Bishop, J.-J. Kim, N. Thompson, D. Chen, Y. Kuru, T. Stefanik and H. L. Tuller, <u>ECS Transactions</u>, 2019, **35**, 1137–1144.
- 15 D. Marrocchelli, S. R. Bishop, H. L. Tuller and B. Yildiz, Advanced Functional Materials, 2012, **22**, 1958–1965.
- 16 S. R. Bishop, D. Marrocchelli, W. Fang, K. Amezawa, K. Yashiro and G. W. Watson, <u>Energy Environmental Science</u>, 2013, **6**, 1142–1146.
- 17 D. Marrocchelli, N. H. Perry and S. R. Bishop, <u>Physical</u> Chemistry Chemical Physics, 2015, **17**, 10028–10039.
- 18 D. Marrocchelli, S. R. Bishop, H. L. Tuller, G. W. Watson and B. Yildiz, <u>Physical Chemistry Chemical Physics</u>, 2012, **14**, 12070–12074.
- 19 N. H. Perry, J. E. Thomas, D. Marrocchelli, S. R. Bishop and H. L. Tuller, ECS Transactions, 2013, **57**, 1879–1884.
- 20 N. H. Perry, S. R. Bishop and H. L. Tuller, Journal of Materials

- Chemistry A, 2014, 2, 18906-18916.
- 21 A. Marthinsen, T. Grande and S. M. Selbach, <u>The Journal of</u> Physical Chemistry C, 2020, **124**, 12922–12932.
- 22 L. O. Anderson, A. X. B. Yong, E. Ertekin and N. H. Perry, Chemistry of Materials, 2021, 33, 8378–8393.
- 23 G. Kresse and J. Hafner, <u>Physical Review B</u>, 1993, **47**, 558–561.
- 24 G. Kresse and J. Hafner, <u>Physical Review B</u>, 1994, **49**, 14251–14269.
- 25 G. Kresse and J. Furthmüller, <u>Physical Review B</u>, 1996, **54**, 11169–11186.
- 26 G. Kresse and J. Furthmüller, <u>Computational Materials</u> Science, 1996, **6**, 15–50.
- 27 P. E. Blöchl, Physical Review B, 1994, 50, 17953-17979.
- 28 G. Kresse and D. Joubert, <u>Physical Review B</u>, 1999, **59**, 1758–1775.
- 29 J. P. Perdew, K. Burke and M. Ernzerhof, <u>Physical Review</u> Letters, 1996, 77, 3865–3868.
- 30 D. Lu and P. Liu, <u>The Journal of Chemical Physics</u>, 2014, **140**, 084101.
- 31 V. I. Anisimov, J. Zaanen and O. K. Andersen, <u>Physical Review</u> <u>B</u>, 1991, **44**, 943–954.
- 32 V. I. Anisimov, F. Aryasetiawan and A. I. Lichtenstein, <u>Journal</u> of Physics: Condensed Matter, 1997, **9**, 767–808.
- 33 A. Staykov, T. Nguyen, T. Akbay and T. Ishihara, <u>The Journal</u> of Physical Chemistry C, 2022, **126**, 7390–7399.
- 34 S. L. Dudarev, G. A. Botton, S. Y. Savrasov, C. J. Humphreys and A. P. Sutton, Physical Review B, 1998, **57**, 1505–1509.
- 35 L. Vasylechko, Y. Pivak, A. Senyshyn, D. Savytskii, M. Berkowski, H. Borrmann, M. Knapp and C. Paulmann, Journal of Solid State Chemistry, 2005, 178, 270–278.
- 36 C. S. Knee, A. Magrasó, T. Norby and R. I. Smith, <u>Journal of</u> Materials Chemistry, 2009, **19**, 3238–3247.
- 37 Z. Ren, B. Yan, J. Liu and J. Zhang, <u>Journal of Rare Earths</u>, 2008, **26**, 331–336.
- 38 K. Momma and F. Izumi, <u>Journal of Applied Crystallography</u>, 2008, **41**, 653–658.
- 39 N. Rosov, J. W. Lynn, Q. Lin, G. Cao, J. W. O'Reilly, P. Pernambuco-Wise and J. E. Crow, Physical Review B, 1992, 45, 982–986.
- 40 Y. Zhang and W. Yang, <u>Physical Review Letters</u>, 1998, **80**, 890–890.
- 41 J. Chase, M. W., <u>Journal of Physical and Chemical Reference</u> <u>Data</u>, 1998, **Monograph 9**, 1–1951.
- 42 N. Fairley, V. Fernandez, M. Richard-Plouet, C. Guillot-Deudon, J. Walton, E. Smith, D. Flahaut, M. Greiner, M. Biesinger, S. Tougaard, D. Morgan and J. Baltrusaitis, Applied Surface Science Advances, 2021, 5, 100112.
- 43 P. Strange, A. Svane, W. M. Temmerman, Z. Szotek and H. Winter, Nature, 1999, 399, 756–758.
- 44 S. T. Pantelides, Z. Y. Lu, C. Nicklaw, T. Bakos, S. N. Rashkeev, D. M. Fleetwood and R. D. Schrimpf, <u>Journal of Non-Crystalline Solids</u>, 2008, **354**, 217–223.
- 45 E. Jedvik, A. Lindman, M. Benediktsson and G. Wahnström,

- Solid State Ionics, 2015, 275, 2-8.
- 46 IUPAC, Compendium of Chemical Terminology, Blackwell Scientific Publications, Oxford, 2nd edn, 1997.
- 47 Z. Hu, R. Meier, C. Schüßler-Langeheine, E. Weschke, G. Kaindl, I. Felner, M. Merz, N. Nücker, S. Schuppler and A. Erb, Physical Review B, 1999, 60, 1460-1463.
- 48 Z. Hu, G. Kaindl, H. Ogasawara, A. Kotani and I. Felner, Chemical Physics Letters, 2000, 325, 241-250.
- 49 T. Higuchi, A. Oda, Y.-S. Liu, P.-A. Glans and J. Guo, Transactions of the Materials Research Society of Japan, 2015, **40**, 37–40.
- 50 E. Holland-Moritz, Zeitschrift für Physik B Condensed Matter, 1992, 89, 285-288.
- 51 M. Nagoshi, Y. Fukuda, N. Yamada, Z. Guo, T. Iri, K. Gondaira, H. Iwasaki, Y. Syono and M. Tachiki, Physical Review B, 1992, **46**, 8635–8637.
- 52 M. Szubka, E. Talik, A. Molak, S. Turczyński and D. A. Pawlak, Crystal Research and Technology, 2010, 45, 1309-1315.

- 53 E. Y. Konysheva and M. V. Kuznetsov, RSC Advances, 2013, 3, 14114-14122.
- 54 J.-S. Kim, C. W. Na, C.-H. Kwak, H.-Y. Li, J. W. Yoon, J.-H. Kim, S.-Y. Jeong and J.-H. Lee, ACS Applied Materials Interfaces, 2019, 11, 25322-25329.
- 55 T. Higuchi, A. Oda, T. Tsuchiya, T. Suetsugu, N. Suzuki, S. Yamaguchi, M. Minohara, M. Kobayashi, K. Horiba and H. Kumigashira, Journal of the Physical Society of Japan, 2015, 84, 114708.
- 56 S. Furuichi, T. Tsuchiya, K. Horiba, M. Kobayashi, M. Minohara, H. Kumigashira and T. Higuchi, Transactions of the Materials Research Society of Japan, 2017, 42, 15-18.
- 57 P. Hartley, R. G. Egdell, K. H. L. Zhang, M. V. Hohmann, L. F. J. Piper, D. J. Morgan, D. O. Scanlon, B. A. D. Williamson and A. Regoutz, The Journal of Physical Chemistry C, 2021, 125, 6387-6400.
- 58 A. V. Krukau, O. A. Vydrov, A. F. Izmaylov and G. E. Scuseria, The Journal of Chemical Physics, 2006, 125, 224106.

# Supporting Information

# Effects of State Filling and Localization on Chemical Expansion in Praseodymium-Oxide Perovskites

Adrian Xiao Bin Yong<sup>1, 2</sup>, Lawrence O. Anderson<sup>1, 2</sup>, Nicola H. Perry<sup>1, 2</sup>, and Elif Ertekin<sup>\*2, 3</sup>

<sup>&</sup>lt;sup>1</sup>Department of Materials Science and Engineering, University of Illinois Urbana-Champaign, Urbana, Illinois, USA

<sup>&</sup>lt;sup>2</sup>Materials Research Laboratory, University of Illinois Urbana-Champaign, Urbana, Illinois, USA

<sup>&</sup>lt;sup>3</sup>Department of Mechanical Science and Engineering, University of Illinois Urbana-Champaign, Urbana, Illinois, USA

<sup>\*</sup>Corresponding author; Email: ertekin@illinois.edu

The projected density of states (PDOS) of stoichiometric  $PrGaO_3$  and  $BaPrO_3$  are as shown in Fig. S1. Note that the energies of each plot have been shifted such that the Fermi level is located at 0 eV. As the U value increases, the occupied Pr-4f states shift left towards the O-2p states, whereas the unoccupied Pr-4f states shift right towards the Pr-5d states.

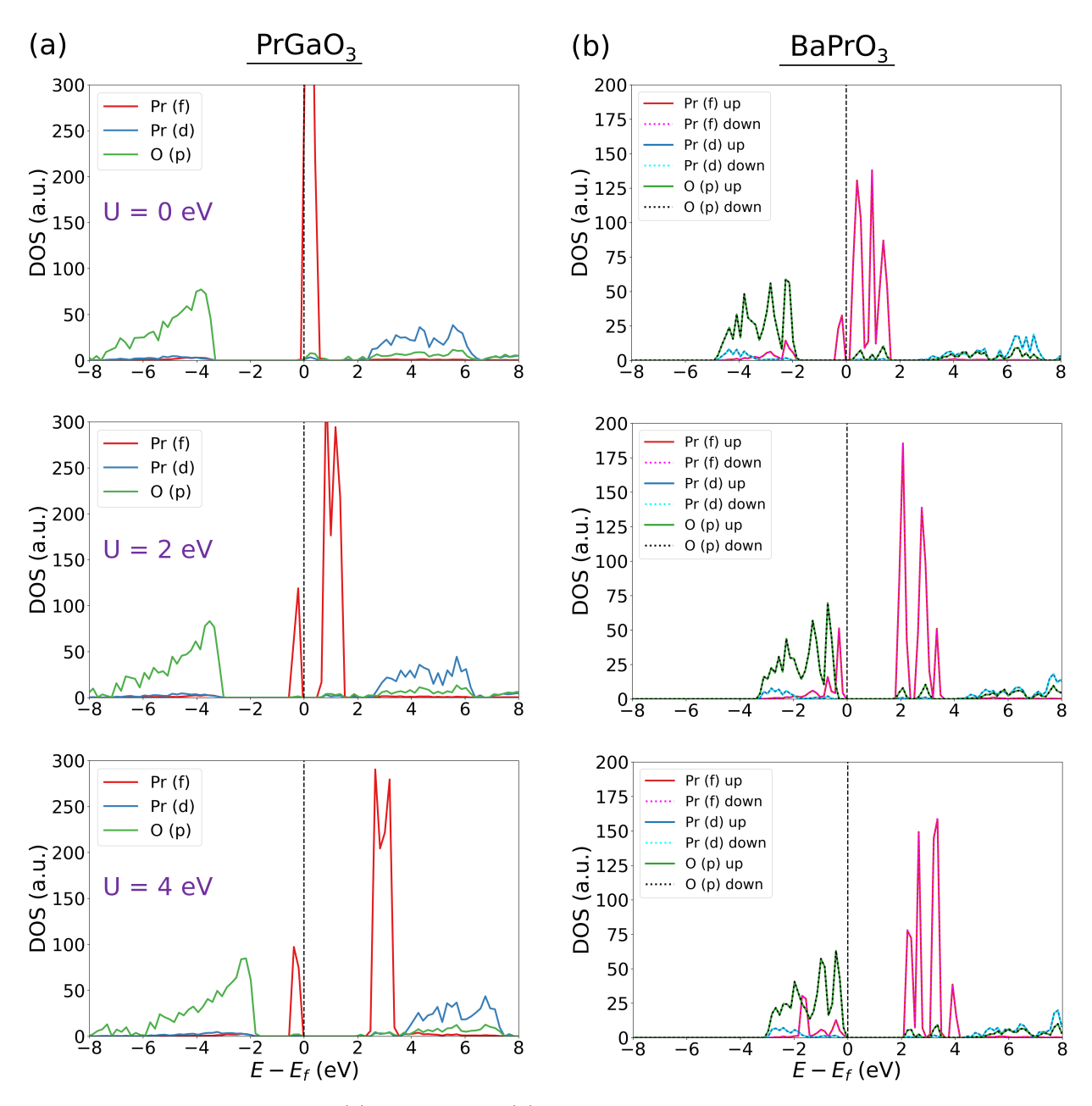


Figure S1: Calculated PDOS of (a)  $PrGaO_3$  and (b)  $BaPrO_3$  for U=0, 2, and 4 eV. The black dashed line represents the Fermi level.

The PDOS of  $PrGa_{0.875}Mg_{0.125}O_{3-\delta}$  (PGM) for  $\delta=0$  and 0.0625 are as shown in Fig. S2. For U=2 eV, the inset shows the enlarged PDOS of the F'-center defect state formed when an O vacancy is introduced to the supercell, which is lower in energy than the Pr-4f hole states.

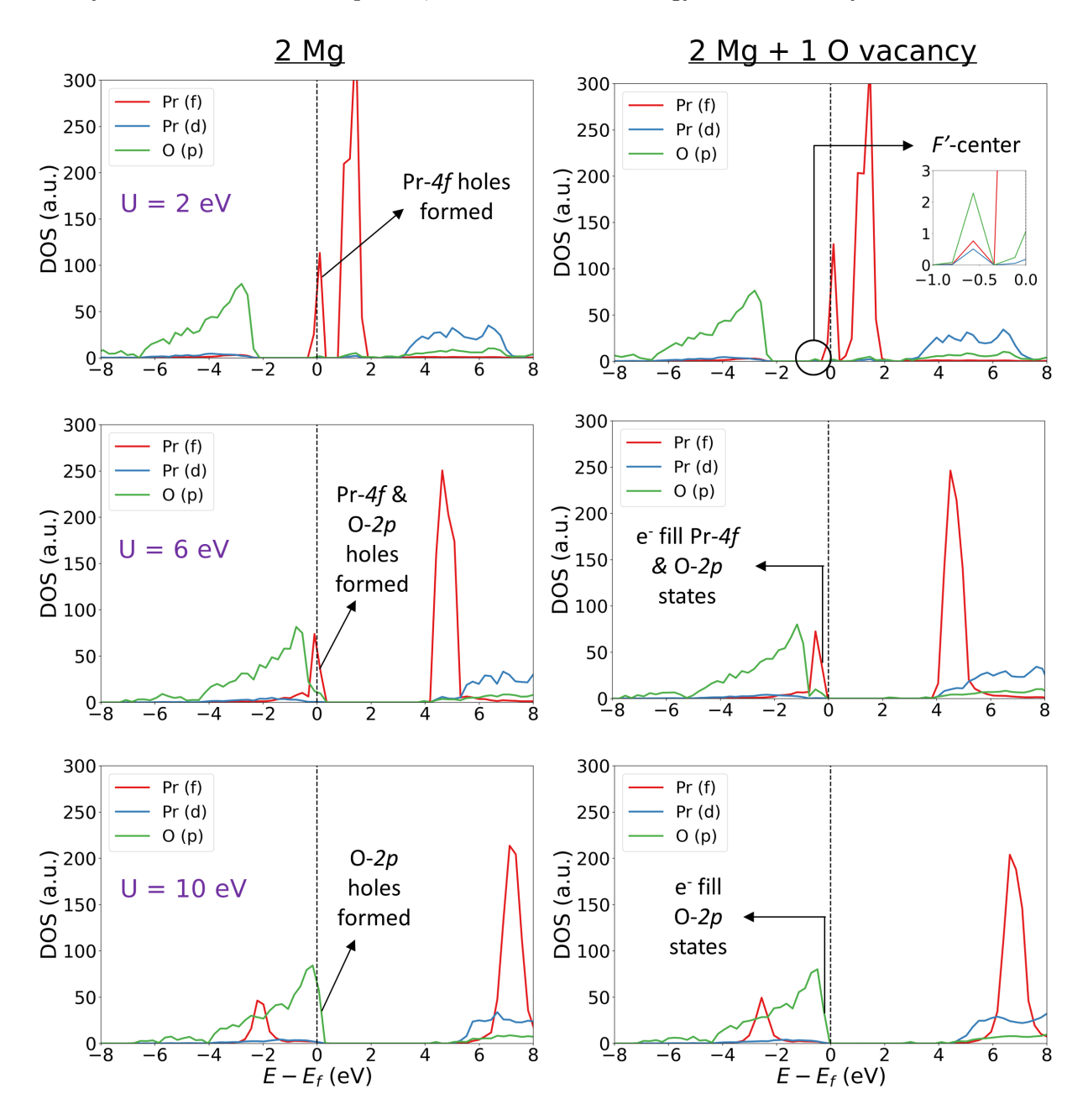


Figure S2: Calculated PDOS of PGM for the supercell with 2 Mg dopants atoms introduced and the supercell with an additional O vacancy added for U=2, 6, and 10 eV. All results are shown for the arrangement where the Mg atoms and O vacancy are far apart. The PDOS of states not shown are negligible in the energy range of the plots.

Table S1 shows the energy difference between the arrangement where the defects are far apart  $(E_{far})$  and the arrangement where the defects are close together  $(E_{close})$  for PGM. Note that the O vacancy was placed far from both Mg dopant atoms in the far arrangement, and between the Mg dopant atoms in the close arrangement. When there are no O vacancies present in PGM, the far arrangement is more energetically favorable by  $\sim 1$  eV per pair of dopants than the close arrangement, as the latter leads to higher strain. When an O vacancy is introduced to PGM, the energy difference decreased to  $\sim 0.2$  eV due to the favorable association between Mg'<sub>Ga</sub> and v<sup>•</sup><sub>O</sub>. However, the far arrangement remained more energetically favorable suggesting that strain effects outweigh the favorable association between the Mg dopants and the O vacancy. If a third case is considered where the Mg dopants are far apart but the O vacancy is located next to one of the Mg dopants, this arrangement will likely be more energetically favorable than the arrangement where all defects are far apart.

Table S1: Energy difference between the far and close arrangements of defects for PGM, when the O vacancy is absent or present

	$E_{far} - E_{close} \text{ (eV)}$	
U (eV)	No O vacancy	1 O vacancy
4	-0.860	-0.170
6	-0.926	-0.250
8	-0.984	-0.233
10	-0.987	-0.236

The PDOS of BaPrO<sub>3- $\delta$ </sub> (BPO) for  $\delta = 0$  and 0.0625 are as shown in Fig. S3.

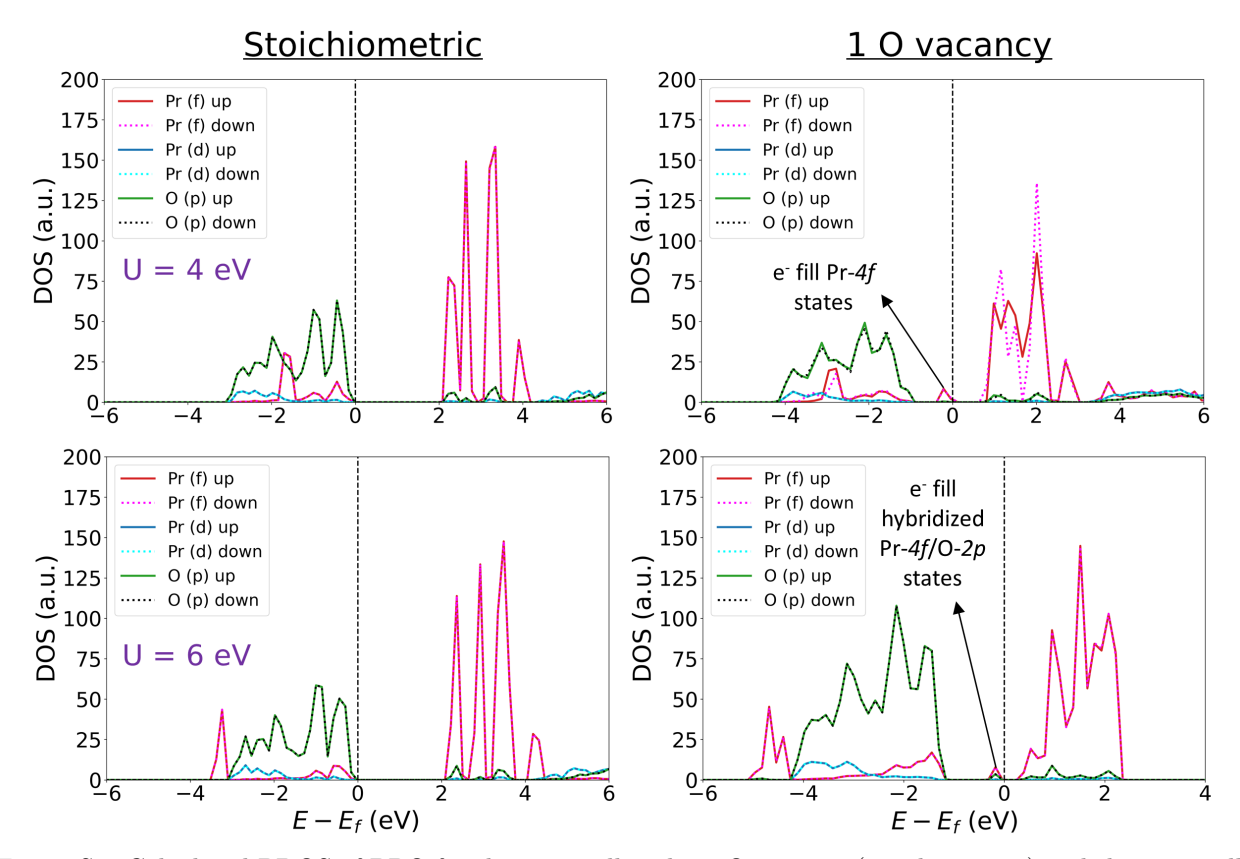


Figure S3: Calculated PDOS of BPO for the supercell with no O vacancy (stoichiometric) and the supercell with one O vacancy added for U=4 and 6 eV. The repeated calculations of BPO for each U value generally yield similar PDOS as shown here.

The PDOS of BaPr<sub>0.875</sub>Y<sub>0.125</sub>O<sub>3- $\delta$ </sub> (BPY) for  $\delta=0$  and 0.0625 are as shown in Fig. S4.

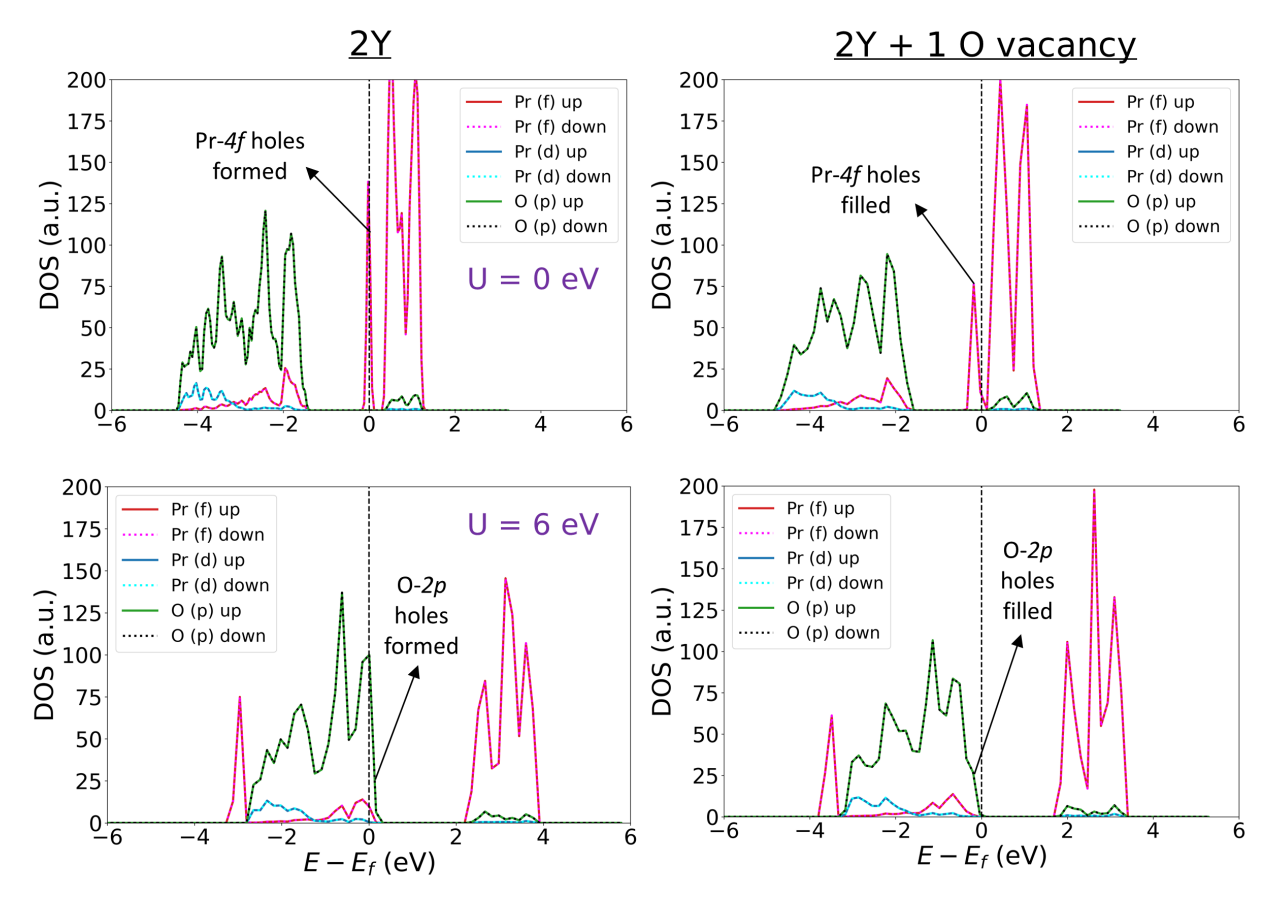


Figure S4: Calculated PDOS of BPY for the supercell with 2 Y dopants atoms introduced and the supercell with an additional O vacancy added for U=0 and 6 eV. All results are shown for the arrangement where the Y atoms and O vacancy are close together.

# Supplementary Note 1. Pr-3d XPS spectra fitting

Quantitative determination of the  $\Pr^{3+}/\Pr^{4+}$  ratio in the surface of our materials requires fitting of the XPS data. In literature concerning Pr oxides, different fitting approaches have been applied  $^{1-3}$ , which for our compositions and data yield different ratios. To our knowledge, two primary fitting approaches have been presented: Method  $1^1$  has been used to determine the amount of  $\Pr^{4+}$  impurity ions in a  $\Pr_x \text{La}_{1-x} \text{AlO}_3$  solid solution. Method  $2^{2,3}$  has been used for  $\Pr_{0,3}$  and two-phase composites composed of a  $(\text{La},\text{Sr},\text{Pr})\text{CoO}_3$  perovskite phase and a  $(\text{La},\text{Sr},\text{Pr})_2\text{CoO}_4$  Ruddlesden-Popper phase. However, to the best of our knowledge, neither method has been used to track changes in  $\Pr_{0,3}$  valence with fixed valence cation substitution or with changes in partial pressure of oxygen (pO2), where the change in  $\Pr_{0,3}$  valence can be reliably predicted in these cases and the validity of the fitting method can be assessed. Also, neither method has been compared to complementary experimental techniques to verify the valence state(s) of  $\Pr_{0,3}$ .

Figure S5 shows our Pr-3d spectra fitted using Method 1 and Method 2. Method 1 assigns the  $4f^2$  and  $4f^3\underline{L}$  peaks as  $\Pr^{3+}$ , and the  $4f^1$  peaks as  $\Pr^{4+}$ . Although the  $4f^1$  peaks indicate the presence of  $\Pr^{4+}$ , the  $4f^2$  and  $4f^3\underline{L}$  peaks may also receive a contribution from  $\Pr^{4+}$  (instead of  $\Pr^{3+}$  only). Method 2 allows the  $4f^2$  and  $4f^3\underline{L}$  peaks to have contributions from both  $\Pr^{3+}$  and  $\Pr^{4+}$ , and the peaks are assigned according to the relative peak positions of reference oxides  $\Pr_2O_3$  ( $\Pr^{3+}$ ) and  $\Pr_2O_3$  (nominally  $\Pr^{4+}$ ). However,  $\Pr_2O_3$  is inappropriate as a reference for  $\Pr^{4+}$  due to covalency in the  $\Pr_2O_3$  spectra of  $\Pr_3O_3$  and the reference oxides, where similar binding-energy shifts (0-1.5 eV) were observed in other mixed  $\Pr_3O_3$  oxides  $P_3O_3$ . These binding-energy shifts may be caused by differences in bond covalency, Madelung energy, and/or final-state relaxation effects  $P_3O_3$ . These significant shifts make the identification of the (up to) 10 highly convoluted peak positions for  $P_3O_3$  and  $P_3O_3$  covalence oxides to quantify  $P_3O_3$  and  $P_3O_3$  and  $P_3O_3$  peaks.

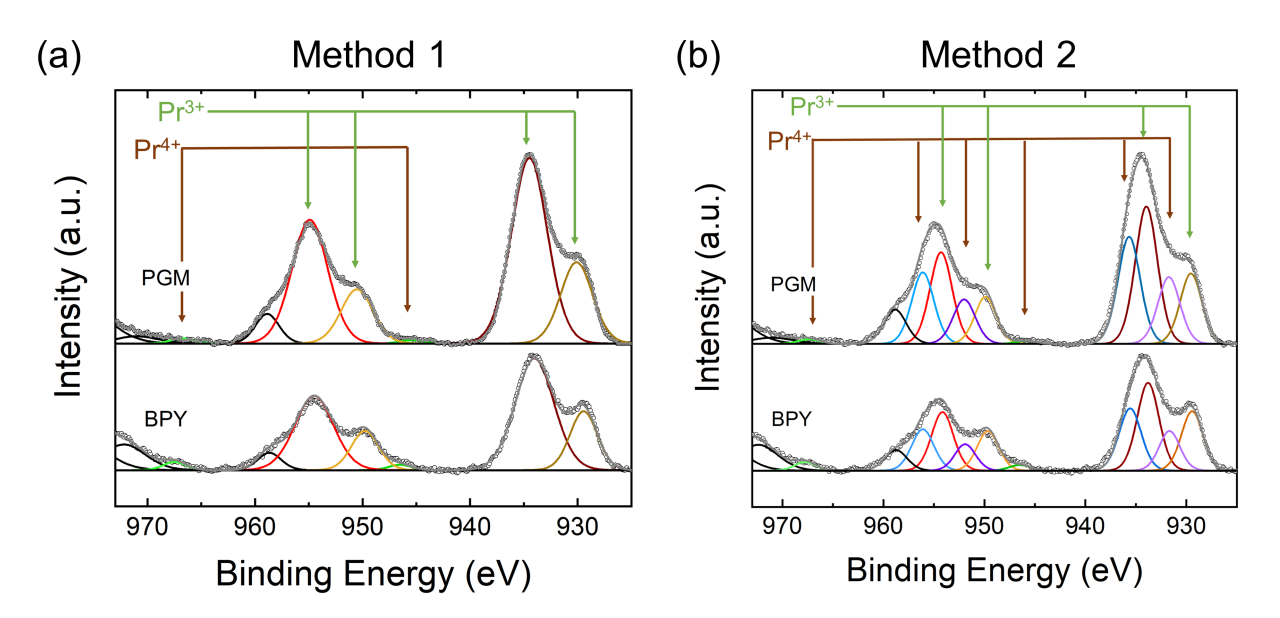


Figure S5: Pr-3d XPS spectra of PGM and BPY fitted using (a) Method 1 and (b) Method 2. Note that the region between 970-980 eV is attributed to O KLL Auger emissions <sup>1,8</sup>.

The fractions of Pr<sup>3+</sup> and Pr<sup>4+</sup> ions were calculated from the fitted peak areas according to Ref. 2 (FWHM fixed to 2.45 eV), and the results for both methods are summarized in Table S2. Method 1 results in mostly Pr<sup>3+</sup> for both materials, with a slightly higher Pr<sup>4+</sup> fraction for BPY. However, the Pr<sup>4+</sup> fraction still appears to be unusually low for BPY, even after taking into account the Pr–O bond covalency in BPY. On the other hand, Method 2 results in much higher Pr<sup>4+</sup> fractions for both materials, and actually shows a higher Pr<sup>4+</sup> fraction for PGM than for BPY. The fraction of Pr<sup>4+</sup> in PGM is unreasonably high, since Pr should exist as mostly Pr<sup>3+</sup> in PGM. Neither fitting method appears to give valence fractions that we can confidently rely on without further experimental verification using methods such as X-ray absorption spectroscopy (XAS). Hence, we chose to perform only a qualitative comparison of the raw spectra instead of using fitted results.

Table S2:  $Pr^{3+}$  and  $Pr^{4+}$  fractions of PGM and BPY, determined from the Pr-3d spectra fitted using Methods 1 and 2

Material	Fitting method	$Pr^{3+}$ fraction	Pr <sup>4+</sup> fraction
PGM	Method 1	0.987	0.013
	Method 2	0.540	0.460
BPY	Method 1	0.969	0.031
	Method 2	0.572	0.428

### Supplementary Note 2. Comparison between XPS valence spectra and DOS

Since we do not observe an isolated (Pr-4f) peak located to the right of the broad (O-2p) feature near the Fermi level of the XPS valence spectra, this indicates that appropriate descriptions of PGM and BPY in DFT+U require  $U \geq 6$  eV and  $U \geq 2$  eV respectively. For these ranges of U values, there is generally good agreement between the XPS valence spectra and the calculated density of states (DOS). Since comparisons were made with the DOS directly without conversion into simulated XPS spectra, some differences in peak widths (peak broadening effects<sup>9</sup> are present in experiments) and peak intensities (the photoelectron spectrum is dependent on the orbital cross sections and excitation energy 10) are expected. The feature at around 12 eV in the BPY XPS spectrum corresponds to the beginning of the Ba-5p peak. However, the small peak at around 9 eV in the BPY XPS spectrum is not present in the calculated DOS. This peak is unlikely to be the Pr-4f peak since photoelectron spectroscopy data of  $BaPrO_3$  from literature  $^{11,12}$  reported Prstates to be located near the top of the O states in the valence band. This discrepancy may have been due to XPS being a surface sensitive technique (~5 nm), whereas the calculated DOS was for the bulk. The coordination environment and possibly composition could be different between the surface and the bulk. Furthermore, BPY was modelled as antiferromagnetic 13 in DFT (0 K), but it should lose its antiferromagnetic ordering at room temperature. These potential differences in surface composition/coordination and magnetism may have led to the observation of the additional peak in the XPS spectrum. However, this peak is far enough below the valence band maximum that it should not influence the formation/location of holes.

Calculations of stoichiometric  $PrGaO_3$  and  $BaPrO_3$  were also performed using the Heyd-Scuseria-Ernzerhof (HSE06) hybrid functional <sup>14</sup>. The orbitals were expanded using a plane wave basis with cutoff energy of 520 eV for both materials.  $PrGaO_3$  was calculated using its unit cell, and the Brillouin zone was sampled using a  $(3 \times 3 \times 3)$  gamma centered k-point grid.  $BaPrO_3$  was calculated using  $2 \times 2 \times 2$  unit cells, initialized with a G-type antiferromagnetic ordering <sup>13</sup>, and the Brillouin zone was sampled using a  $(2 \times 2 \times 2)$  Monkhorst-Pack k-point grid. Structural relaxations were performed, allowing the cell shape, cell volume, and atom positions to relax, until the force on each atom was below 0.01 eV/Å.

The PDOS for both materials are as shown in Fig. S6. Based on the relative positions of the Pr-4f and O-2p states in the valence band, the PDOS calculated using HSE06 appear to match those calculated using PBE and U=4 eV for both PGO and BPO (see Fig. S1), apart from the underestimated band gap for PBE. Although the Hubbard U correction was only applied to the Pr-4f states in PBE+U, the Pr-5d states still match well with HSE06 and do not appear to be overly delocalized. Our experimental valence band XPS spectra showed that the Pr-4f peak in the valence band is not an isolated peak located to the right of the O-2p states, indicating that HSE06 still does not describe  $PrGaO_3$  correctly despite being a higher level of theory.

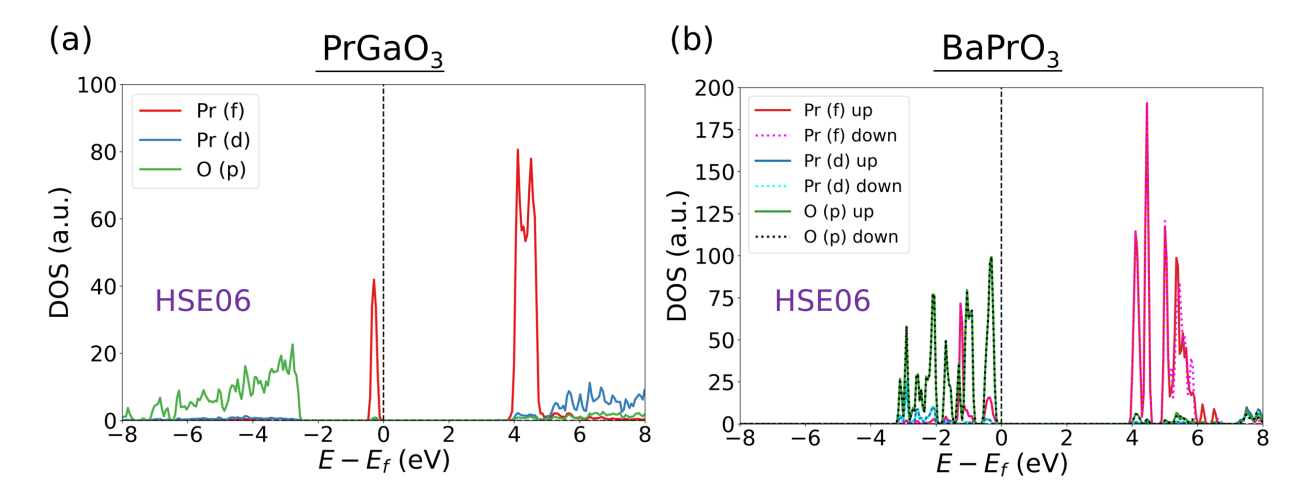


Figure S6: Calculated PDOS of (a) PrGaO<sub>3</sub> and (b) BaPrO<sub>3</sub> using the HSE06 hybrid functional.

The strain along the a-, b-, and c-axis for PGM when one O vacancy is introduced is shown in Fig. S7. PGM is orthorhombic and demonstrates an anisotropic chemical expansion, where the expansion is the largest along the a-axis, followed by the c-axis, and is accompanied by a contraction along the b-axis. This anisotropic expansion is consistent across all U values regardless of which hole states are filled, and matches our previously reported experimental measurements  $^{15}$ .

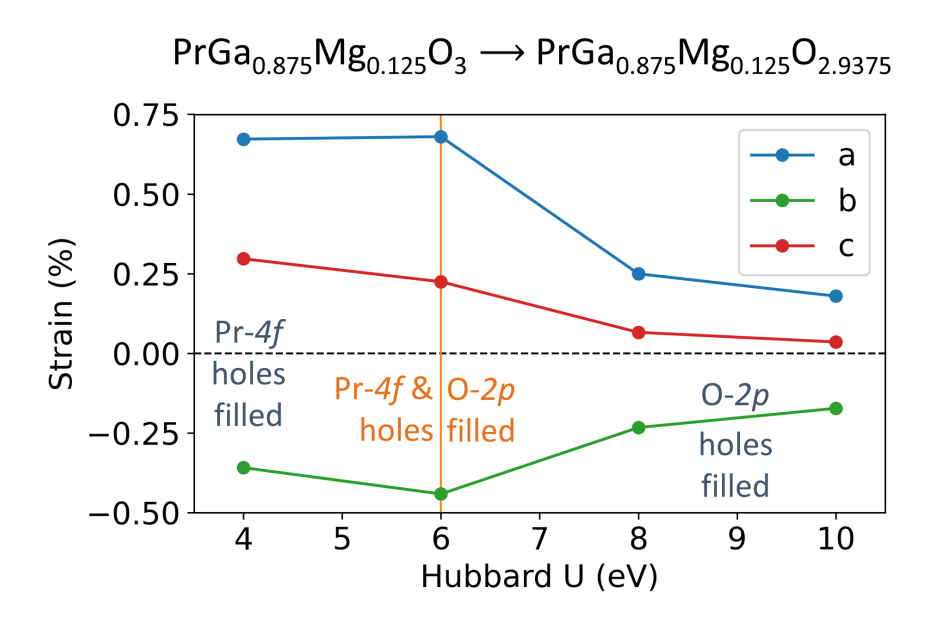


Figure S7: Plot of percentage strain as a function of Hubbard U for introducing one O vacancy to  $PrGa_{0.875}Mg_{0.125}O_3$ .

## References

- M. Szubka, E. Talik, A. Molak, S. Turczyński and D. A. Pawlak, Crystal Research and Technology, 2010, 45, 1309–1315.
- [2] E. Y. Konysheva and M. V. Kuznetsov, RSC Advances, 2013, 3, 14114–14122.
- [3] J.-S. Kim, C. W. Na, C.-H. Kwak, H.-Y. Li, J. W. Yoon, J.-H. Kim, S.-Y. Jeong and J.-H. Lee, *ACS Applied Materials Interfaces*, 2019, **11**, 25322–25329.
- [4] S. G. Minasian, E. R. Batista, C. H. Booth, D. L. Clark, J. M. Keith, S. A. Kozimor, W. W. Lukens, R. L. Martin, D. K. Shuh, S. C. E. Stieber, T. Tylisczcak and X.-d. Wen, *Journal of the American Chemical Society*, 2017, 139, 18052–18064.
- [5] S. K. Pandey, R. Bindu, P. Bhatt, S. M. Chaudhari and A. V. Pimpale, Physica B: Condensed Matter, 2005, 365, 47–54.
- [6] E. Poggio-Fraccari, G. Baronetti and F. Mariño, Journal of Electron Spectroscopy and Related Phenomena, 2018, 222, 1–4.
- [7] M. J. Guittet, J. P. Crocombette and M. Gautier-Soyer, *Physical Review B*, 2001, **63**, 125117.
- [8] B. Demri and D. Muster, Journal of Materials Processing Technology, 1995, 55, 311–314.
- [9] P. S. Bagus, E. S. Ilton and C. J. Nelin, Surface Science Reports, 2013, 68, 273–304.
- [10] M. Bagheri and P. Blaha, Journal of Electron Spectroscopy and Related Phenomena, 2019, 230, 1–9.
- [11] T. Higuchi, A. Oda, T. Tsuchiya, T. Suetsugu, N. Suzuki, S. Yamaguchi, M. Minohara, M. Kobayashi, K. Horiba and H. Kumigashira, *Journal of the Physical Society of Japan*, 2015, 84, 114708.
- [12] S. Furuichi, T. Tsuchiya, K. Horiba, M. Kobayashi, M. Minohara, H. Kumigashira and T. Higuchi, *Transactions of the Materials Research Society of Japan*, 2017, **42**, 15–18.
- [13] N. Rosov, J. W. Lynn, Q. Lin, G. Cao, J. W. O'Reilly, P. Pernambuco-Wise and J. E. Crow, Physical Review B, 1992, 45, 982–986.
- [14] A. V. Krukau, O. A. Vydrov, A. F. Izmaylov and G. E. Scuseria, *The Journal of Chemical Physics*, 2006, **125**, 224106.
- [15] L. O. Anderson, A. X. B. Yong, E. Ertekin and N. H. Perry, Chemistry of Materials, 2021, 33, 8378–8393.